Citation: Cell Death and Disease (2013) 4, e465; doi:10.1038/cddis.2012.201

www.nature.com/cddis

TNF can activate RIPK3 and cause programmed necrosis in the absence of RIPK1

DM Moujalled[1,2], WD Cook[3], T Okamoto[4], J Murphy[1,2], KE Lawlor[1,2], JE Vince[1,2] and DL Vaux*[,1,2]

Ligation of tumor necrosis factor receptor 1 (TNFR1) can cause cell death by caspase 8 or receptor-interacting protein kinase 1 (RIPK1)- and RIPK3-dependent mechanisms. It has been assumed that because RIPK1 bears a death domain (DD), but RIPK3 does not, RIPK1 is necessary for recruitment of RIPK3 into signaling and death-inducing complexes. To test this assumption, we expressed elevated levels of RIPK3 in murine embryonic fibroblasts (MEFs) from wild-type (WT) and gene-deleted mice, and exposed them to TNF. Neither treatment with TNF nor overexpression of RIPK3 alone caused MEFs to die, but when levels of RIPK3 were increased, addition of TNF killed WT, *Ripk1*$^{-/-}$, *caspase* 8$^{-/-}$, and *Bax*$^{-/-}$/*Bak*$^{-/-}$ MEFs, even in the presence of the broad-spectrum caspase inhibitor Q-VD-OPh. In contrast, *Tnfr1*$^{-/-}$ and *Tradd*$^{-/-}$ MEFs did not die. These results show for the first time that in the absence of RIPK1, TNF can activate RIPK3 to induce cell death both by a caspase 8-dependent mechanism and by a separate Bax/Bak- and caspase-independent mechanism. RIPK1 is therefore not essential for TNF to activate RIPK3 to induce necroptosis nor for the formation of a functional ripoptosome/necrosome.
Cell Death and Disease (2013) **4,** 465; doi:10.1038/cddis.2012.201; published online 17 January 2013
Subject Category: Experimental Medicine

By binding to tumor necrosis factor receptor 1 (TNFR1), TNF can activate both transcription factors, such as AP-1 and NF-κB, as well as cell death mechanisms.[1] Because most cell lines are not killed by the addition of TNF alone, but many die when TNF is added together with inhibitors of transcription or translation, such as actinomycin D or cycloheximide (CHX),[2] these transcription factor pathways appear to promote cell survival. Consistent with this notion, cell lines mutant for the p65/RelA component of NF-κB are killed by TNF alone.[3] These observations show that upon ligation, TNFR1 not only activates the NF-κB pathway but also triggers cell death pathways that can be blocked by an NF-κB-dependent process.

TNF activates a number of different death mechanisms depending of the cell type and circumstances. In many cell types, including mouse embryonic fibroblasts (MEFs), cell death triggered by TNF (plus CHX), or by related ligands such as TRAIL or FasL, requires the presence of the adaptor protein Fas-associated death domain (FADD) and the protease caspase 8.[4,5] The receptors for these ligands bear cytoplasmic death domains (DDs) that allow them to bind directly or indirectly to FADD, which in turn binds to the death effector domains of procaspase 8, causing it to activate.[6]

Although cell death triggered by ligation of death receptors can often be blocked by the caspase 8 inhibitor crmA[7,8] or by pancaspase inhibitory compounds such as Q-VD-OPh[9] or z-VAD-FMK,[10] not all cells are protected. For example, murine fibrosarcoma L929 cells were killed more efficiently by TNF in the presence of z-VAD-FMK,[11,12] and z-VAD-FMK did not prevent the death of U937 cells treated with TNF, or HT29 cells treated with TNF plus an inhibitor of apoptosis protein (IAP) antagonist (smac-mimetic).[13] Instead, these cells died displaying a characteristic appearance termed 'necroptosis'.[11]

Necroptosis, or programmed necrosis, refers to a caspase 8-independent death mechanism triggered by the receptor-interacting protein kinase 1 and 3 (RIPK1 and RIPK3).[11,14–18] Necroptosis is thought to be dependent on the enzymatic activity of RIPK1, as suggested by the protection conveyed by the RIPK1 kinase inhibitor necrostatin.[19] Because RIPK1, but not RIPK3, bears a DD that can interact with the TNFR1,[20] it has been suggested that upon binding of TNF, RIPK1 is recruited to TNFR1 either directly via its DD or indirectly by a DD-bearing adaptor, such as TNF receptor-associated death domain (TRADD), to form a complex on the cytoplasmic domain of TNFR1.[21] In cells destined to die, this complex is released from TNFR1, and recruits other proteins, such as FADD and caspase 8 to induce apoptosis, or interacts with RIPK3 to cause necroptosis.[22,23] RIPK1 is thought to have a crucial role in recruiting RIPK3 by binding via their shared RIP homotypic interaction motifs (RHIMs).[22,24,25] Therefore, according to this model, RIPK1 recruitment of RIPK3 is essential for ligated TNFR1 to signal necroptosis.[26,27]

[1]The Walter and Eliza Hall Institute of Medical Research, 1G Royal Parade, Melbourne, Victoria, Australia; [2]Department of Medical Biology, The University of Melbourne, Parkville, Victoria, Australia; [3]Department of Biochemistry, La Trobe Institute for Molecular Science, La Trobe University, Kingsbury Drive Bundoora, Melbourne, Victoria, Australia and [4]Department of Molecular Virology, Research Institute for Microbial Diseases, Osaka University, Yamadaoka, Suita, Osaka, Japan
*Corresponding author: DL Vaux, Department of Biochemistry, La Trobe Institute for Molecular Science, La Trobe University, Kingsbury Drive Bundoora, Melbourne, Victoria 3086, Australia. Tel: +61 3 9345 4129; E-mail: vaux@wehi.edu.au
Keywords: TNF; necroptosis; receptor-interacting protein kinases; smac-mimetic; inhibitor of apoptosis proteins TNF
Abbreviations: CHX, cycloheximide; DD, death domain; TNF, tumor necrosis factor; TNFR1, TNF receptor 1; RIPK1/3, receptor-interacting protein kinases; IAPs, inhibitor of apoptosis proteins; TRADD, TNF receptor-associated death domain; FADD, Fas-associated death domain
Received 28.11.12; accepted 4.12.12; Edited by G Melino

To determine the roles and requirements for TRADD, FADD, caspase 8, RIPK1, RIPK3, and Bax/Bak for TNF-induced cell death, we derived MEFs from gene-deleted mice, and treated them with TNF, in the presence or absence of exogenously expressed RIPK3. We found that addition of TNF activated both caspase 8- and RIPK3-dependent death pathways, even in the absence of RIPK1. Our results show that although TNFR1 and TRADD were necessary for TNF to activate RIPK3 to cause cell death, RIPK1 and FADD were not.

Results

Elevation of RIPK3 allows TNF to cause death of MEFs. To determine whether overexpression of RIPK3 alone was sufficient to cause death of MEFs, we infected wild-type (WT) MEFs with a 4-hydroxytamoxifen (4HT)-inducible lentiviral vector expressing FLAG-tagged RIPK3 (Figure 1a). As expected, in the absence of 4HT, cells treated with TNF for 24 h did not die, whereas those treated with TNF plus a smac-mimetic compound, which depletes cells of cIAP1,[7] did die (Figure 1b, upper panels). Induction of FLAG-RIPK3 by 4HT also failed to kill the cells, but when TNF was added to cells in which FLAG-RIPK3 had been induced, they died (Figure 1b, lower panels). These results show that although elevation of RIPK3 levels alone is not sufficient to cause cell death, it can sensitize MEFs to killing by TNF, even when cIAP1 is present.

TNFR1 and TRADD are required for TNF to cause death of MEFs with elevated RIPK3. TNFR1 signaling involves formation of two distinct signaling complexes, the transient membrane-associated TNFR1 signaling complex (complex I) and the cytoplasmic signaling complex termed complex II.[21] To determine components required for TNF to cause death of cells expressing elevated RIPK3, we tested MEF lines that were mutant for proteins implicated in TNF signaling. We infected *Tnfr1*$^{-/-}$, *Tnfr2*$^{-/-}$, and *Tradd*$^{-/-}$ MEFs with the inducible lentiviral vector expressing FLAG-tagged RIPK3 (Supplementary Figure 1a).

Unlike WT MEFs and those mutant for TNFR2, the *Tnfr1*$^{-/-}$ and *Tradd*$^{-/-}$ MEFs were not killed when RIPK3 expression was induced with 4HT and TNF was added (Figure 2). Therefore, both TNFR1 and TRADD are required for TNF to activate RIPK3's killing function.

TNF can activate RIPK3 and cause cell death in the absence of caspase 8 and RIPK1. Numerous reports have described 'programmed necrosis' or 'necroptosis' as forms of cell death mediated by the serine/threonine kinases RIPK1 and RIPK3 that are independent of caspase 8.[11,14,18] To determine whether TNF-triggered death of cells with elevated RIPK3 required caspase 8, we generated *caspase 8*$^{-/-}$ MEFs by deleting loxP-flanked caspase 8 alleles *in vitro* (Supplementary Figure 1b), and then infected them with the 4HT-inducible RIPK3 lentivirus.

First, we compared the sensitivity of WT, *caspase 8*$^{-/-}$, and *Ripk1*$^{-/-}$ MEFs to killing by TNF plus smac-mimetic (Figure 3a). Unlike WT MEFs, which were efficiently killed by TNF plus smac-mimetic, very few of the *Ripk1*$^{-/-}$ and *caspase 8*$^{-/-}$ cells died, indicating that when IAPs are depleted by smac-mimetic, TNF triggers death of MEFs by a RIPK1- and caspase 8-dependent mechanism.[28,29] This requirement of RIPK1 and caspase 8 for killing of MEFs by TNF plus smac-mimetic is similar to that observed in neuroblastoma cells treated with TRAIL and IAP inhibitor.[30]

To determine whether TNF-triggered death of MEFs with elevated RIPK3 used the same mechanism as when TNF caused death of IAP-depleted cells, we infected the *caspase 8*$^{-/-}$ and *Ripk1*$^{-/-}$ MEFs with the inducible

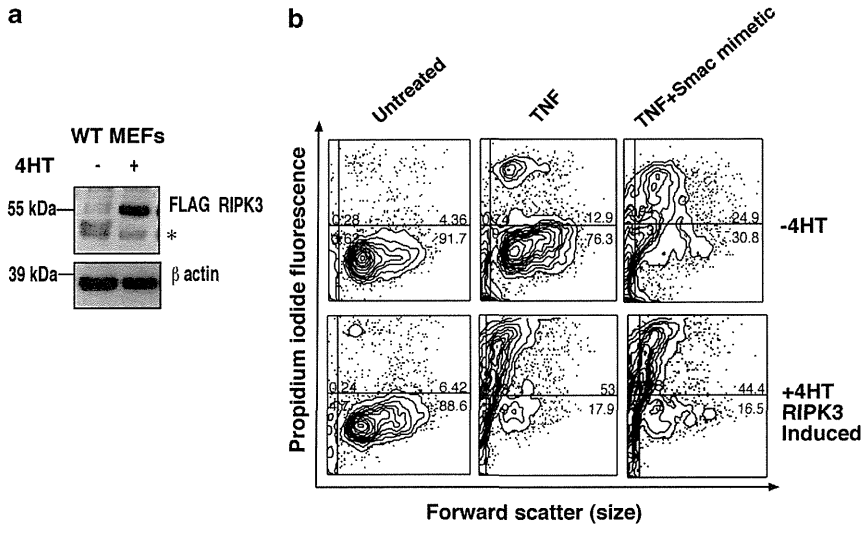

Figure 1 TNF causes death of cells with elevated RIPK3. (**a**) WT MEFs were infected with a lentiviral vector-expressing FLAG RIPK3. Cells were induced with 10 nM 4HT for 24 h, and lysates were probed for FLAG. β-Actin was used as a loading control. *, indicates a nonspecific band. (**b**) Expression of FLAG-RIPK3 in MEFs was induced with 10 nM 4HT for 24 h (lower panels), and cells were then treated with 100 ng/ml TNF or TNF plus 500 nM smac-mimetic for a further 24 h. Cells were stained with PI and analyzed by flow cytometry to detect loss of plasma membrane integrity

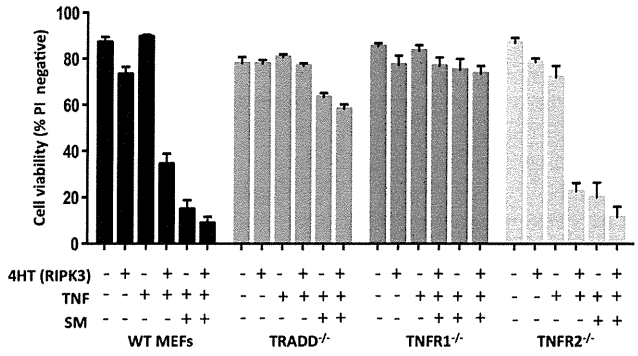

Figure 2 TNFR1 and TRADD are necessary for TNF to cause death of MEFs treated with smac-mimetic or with elevated RIPK3. FLAG-RIPK3 was induced in WT, *Tnfr1*$^{-/-}$, *Tnfr2*$^{-/-}$, and *Tradd*$^{-/-}$ MEFs with 10 nM 4HT for 24 h. Cells were then treated with 100 ng/ml TNF or TNF plus 500 nM smac-mimetic for a further 24 h, stained with PI, and analyzed by flow cytometry. Columns show mean ± S.E.M., where $n = 3$ independently performed experiments

lentiviral vector bearing FLAG-tagged RIPK3 (Figure 3b and Supplementary Figure 1c). When FLAG-RIPK3 was induced in *Ripk1*$^{-/-}$ and *caspase 8*$^{-/-}$ MEFs, little cell death occurred (Figure 3c). There was also little cell death when TNF was added alone. However, addition of TNF to cells in which RIPK3 had been induced by 4HT strongly induced cell death, both in short-term (Figure 3c) and long-term clonogenic survival assays (Figure 3d). Therefore, neither RIPK1 nor caspase 8 is required for TNF to induce cell death when RIPK3 levels are elevated, but both are needed for TNF to kill cells in which IAPs are depleted by a smac-mimetic (Figure 3b). This indicates that while death of MEFs caused by TNF plus smac-mimetic requires both RIPK1 and caspase 8 activity, when RIPK3 levels are elevated, TNF can induce a RIPK1- and caspase 8-independent death mechanism.

RIPK3 killing triggered by TNF does not require Bax/Bak. Although several groups have shown that RIPK1 and RIPK3 can trigger a caspase-independent, necrotic form of cell death, a number of different effector mechanisms have been proposed. For example, it has been reported that in some cells, RIP kinases cause cell death by stimulating production of reactive oxygen species (ROS) or by disrupting mitochondrial integrity.[14] In addition, Zhang *et al.*[18] suggested that RIPK3 generates ROS by interacting with the mitochondrial metabolic enzymes glutamate dehydrogenase and glycogen phosphorylase, whereas another group proposed that RIPK3 induces cell death by interacting with MLKL and PGAM5, and activating DRP-1 to cause mitochondrial dysfunction;[17,22] a fourth group found that binding to DNA-dependent activator of interferon regulatory factors (DAI) was necessary for RIPK3 to cause necrosis;[31] and a fifth group reported that Bax or Bak was necessary for TNF-induced necrosis.[32] To determine whether RIPK3 causes cell death by activating the intrinsic (Bax/Bak-dependent) pathway, we infected *Bax*$^{-/-}$/*Bak*$^{-/-}$ MEFs with an inducible lentiviral vector encoding FLAG RIPK3 (Supplementary Figure 1d), and treated the cells with TNF. As shown in Figure 4, when RIPK3 levels were elevated, TNF caused a similar amount of death of *Bax*$^{-/-}$/*Bak*$^{-/-}$ as of WT MEFs, indicating that activated RIPK3 can kill cells by a Bax/Bak-independent mechanism. Furthermore, as the broad-spectrum caspase inhibitor Q-VD-OPh was not able to prevent death of the *Bax*$^{-/-}$/*Bak*$^{-/-}$ MEFs, RIPK3 must be able to activate a death mechanism that is not only independent of Bax and Bak but also does not require caspase activity.

When RIPK3 levels are elevated, TNF activates caspases whether RIPK1 is present or not. Even though it was clear that when RIPK3 levels were elevated, TNF could trigger cell death by a caspase 8-independent mechanism (Figures 3c and d), TNF is also capable of activating caspase 8, because when IAPs were depleted by smac-mimetic, TNF killed WT, but not *caspase 8*$^{-/-}$ cells (Figures 3c and d). To see whether TNF could activate caspase 8 when RIPK3 levels were elevated, we treated WT and *Ripk1*$^{-/-}$ MEFs with 4HT to induce FLAG-RIPK3, added TNF, and after 4 h lysed the cells and analyzed them by western blot (Figure 5a). Addition of TNF was able to trigger processing of caspase 8, but only when FLAG-RIPK3 was induced. Strikingly, caspase 8 processing was triggered by the addition of TNF both in the WT and *Ripk1*$^{-/-}$ MEFs, indicating that when RIPK3 levels are elevated, TNFR1 can signal via RIPK3 to activate caspase 8 even in the absence of RIPK1.

To further analyze the caspase pathways that were activated by TNF in cells with elevated RIPK3, we performed additional experiments in *Ripk1*$^{-/-}$ and *caspase 8*$^{-/-}$ MEFs, using western blots to test for processing of caspase 3 and cleavage of PARP, and taking cells from duplicate wells to assess their viability by flow cytometry.

As shown in Figure 5b, TNF triggered the processing and activation of caspase 3 and PARP cleavage only in cells with elevated RIPK3. Furthermore, when RIPK3 was elevated, TNF caused activation of caspase 3 in *Ripk1*$^{-/-}$ MEFs, but not in *caspase 8*$^{-/-}$ MEFs.

Taken together, these experiments show that when ligated, TNFR1 can signal to RIPK3 independently of RIPK1, and if its levels are high enough, RIPK3 can activate caspase 8 and caspase 3 even if RIPK1 is absent. Nevertheless, activated caspase 8 was not required for most of the death when TNF was added to cells with elevated RIPK3, because Q-VD-OPh was not able to prevent their death (Figure 5c, WT and *Ripk1*$^{-/-}$ gray columns), and cell death still occurred even in the *caspase 8*$^{-/-}$ MEFs (Figure 5c, light gray columns).

TNF can activate RIPK3 in the absence of FADD. To determine whether FADD was required for TNFR1 to activate RIPK3, we transfected the RIPK3-inducible construct into *Fadd*$^{-/-}$ MEFs. When these cells were treated with 4HT (to induce RIPK3) and TNF, they did not die. However, as western blots showed that the *Fadd*$^{-/-}$ MEFs expressed relatively low levels of MLKL, a protein thought to be necessary for RIPK3-induced cell death,[22,33] we hypothesized that the *Fadd*$^{-/-}$ MEFs might be surviving because of low levels of MLKL, rather than because they lacked FADD. To resolve this, we transfected the *Fadd*$^{-/-}$ cells with a second vector bearing a doxycycline-inducible MLKL construct (Figure 6a). Addition of TNF to *Fadd*$^{-/-}$ cells

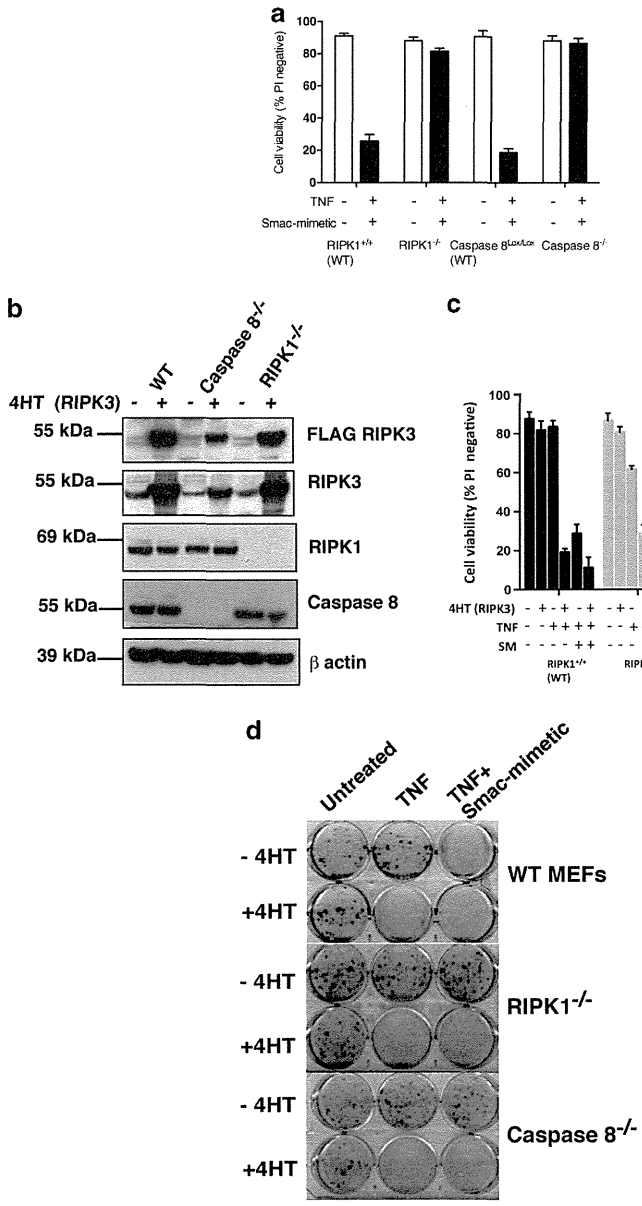

Figure 3 Both caspase 8 and RIPK1 are required for TNF plus smac-mimetic to cause cell death, but when levels of RIPK3 are elevated, TNF alone can induce cell death in the absence of caspase 8 or RIPK1. (**a**) MEF lines were untreated (white bars) or treated with 100 ng/ml TNF plus 500 nM smac-mimetic (black bars) for 24 h. Cell viability was determined by PI exclusion using a flow cytometer. Columns show mean ± S.E.M., where $n = 3$ independently performed experiments. (**b**) WT, *caspase* $8^{-/-}$, and *Ripk1* $^{-/-}$ MEFs bearing the inducible FLAG RIPK3 vector were untreated or treated with 10 nM 4HT for 24 h, and lysates were probed with antibodies to reveal levels of endogenous or induced FLAG-tagged proteins. (**c**) Cell lines were induced with 10 nM 4HT for 24 h, and then treated, where indicated, with 100 ng/ml TNF and 500 nM smac-mimetic (SM) for a further 24 h, and viability determined by flow cytometric analysis of PI exclusion. Columns show mean ± S.E.M., where $n = 3$ independently performed experiments. (**d**) Cell lines were induced with 10 nM 4HT for 24 h and cultured with 100 ng/ml TNF alone or TNF plus 500 nM smac-mimetic for 48 h. Cells were resuspended using trypsin, re-plated, and after 5 days stained with crystal violet to assess clonogenicity

in which both RIPK3 and MLKL were induced increased the amount of cell death (Figure 6b). Therefore, in these cells ligated TNFR1 was able to activate RIPK3 and MLKL in the absence of FADD. Furthermore, we could show upon induction of RIPK3, MLKL, and TNF treatment, there was no caspase 8 cleavage in the *Fadd*$^{-/-}$ MEFs as compared to WT MEFs with RIPK3 overexpression and TNF treatment (Figure 6c). Therefore, in order for RIPK3 to induce activation and cleavage of caspase 8, it requires FADD.

Discussion

We set out to determine the requirements for particular signaling components involved in cell death in response to TNF. To do so, we used MEFs derived from gene-deleted mice. Consistent with many earlier reports, addition of TNF to WT MEFs did not cause them to die,[29,34] but when the cells had been treated with a smac-mimetic compound that depletes cells of cIAP1, addition of TNF did cause cell death.

As TNF plus smac-mimetic did not kill *Ripk1*$^{-/-}$ or *caspase 8*$^{-/-}$ MEFs, which were able to divide and form colonies, cIAP1 in WT MEFs must prevent activation of a TNF-induced death pathway that requires both RIPK1 and caspase 8.

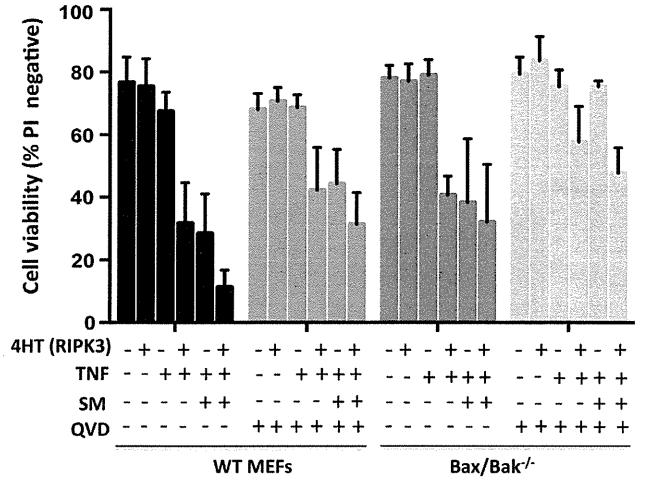

Figure 4 Death induced by TNF and activated RIPK3 is independent of proapoptotic Bcl-2 family proteins Bax and Bak. WT and *Bax*$^{-/-}$/*Bak*$^{-/-}$ MEFs bearing the inducible FLAG-RIPK3 vector were induced with 10 nM 4HT for 24 h. Where indicated, cells were pretreated with 10 μM Q-VD-OPh for 1 h and subsequently treated with 100 ng/ml TNF or TNF plus 500 nM smac-mimetic (SM) for 24 h. Cells were stained with PI and cell viability determined by flow cytometry. Columns show mean ± S.E.M., where $n = 3$ independently performed experiments

Although the MEF lines expressed endogenous RIPK3, to determine if overexpression of RIPK3 alone was sufficient to induce necroptosis, we expressed additional RIPK3 from an inducible lentiviral vector. Overexpression of RIPK3 alone was not sufficient to cause death of MEFs, but unlike WT cells, cells with increased RIPK3 died upon addition of TNF. We found that when RIPK3 levels were increased, TNF triggered activation of caspase 8, whether RIPK1 was present or not. These results show that when ligated, TNFR1 can activate RIPK3, and thereby cause activation of caspases 8 and 3, cleavage of PARP, and cell death, even when RIPK1 was absent.

These findings question prior assumptions that because it bears a DD, RIPK1 was essential for TNF to induce activation of RIPK3, or was essential for TNF to activate caspase 8. Although we do not know precisely how TNFR1 activates RIPK3 in the absence of RIPK1, TRADD appears to be necessary, but to date there have been no reports showing that TRADD can bind to RIPK3. TRAF2 might also be responsible for recruiting RIPK3 into death-inducing complexes, as TRAF2 is rapidly recruited to complex I upon ligation of TNFR1, and RIPK3 has been reported to co-immunopreciptitate with TRAF2.[35]

We initially wondered if FADD might be responsible for recruiting RIPK3 to death-inducing complexes in the *Ripk1*$^{-/-}$ MEFs, firstly because some preliminary experiments suggested that *Fadd*$^{-/-}$ MEFs did not die when RIPK3 was elevated and cells were treated with TNF, and secondly because it has been reported that FADD can interact directly with RIPK3.[14,23] However, the *Fadd*$^{-/-}$ line had relatively low

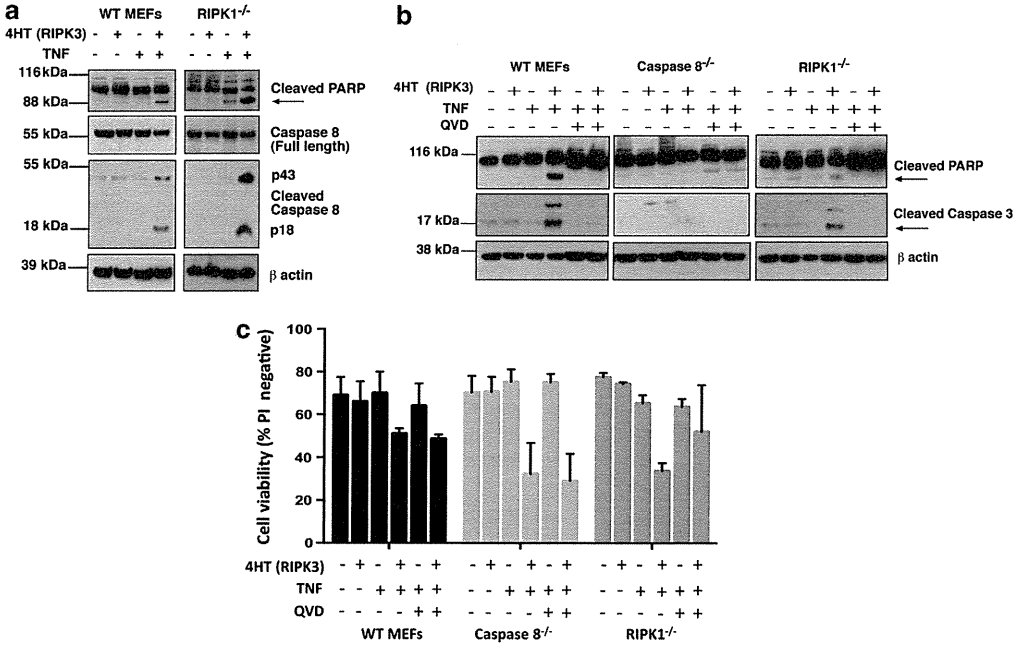

Figure 5 TNF treatment of cells overexpressing RIPK3 activates caspases, but this is not necessary for cell death. (**a**) WT and *Ripk1*$^{-/-}$ MEFs were induced with 10 nM 4HT for 24 h and treated with 100 ng/ml TNF. After 4 h, cells were harvested, lysed, and analyzed by western blotting, and probed for poly (ADP-ribose) polymerase (PARP) and both full-length and cleaved caspase 8. β-Actin was used as a loading control. (**b**, **c**) WT (*caspase 8*$^{lox/lox}$), *caspase 8*$^{-/-}$, and *Ripk1*$^{-/-}$ MEFs in duplicate wells were induced with 10 nM 4HT for 24 h and treated with 100 ng/ml TNF. (**b**) After 4 h, cells from one set of wells were harvested, lysed, and analyzed by western blot probed for PARP and cleaved caspase 3. (**c**) After 4 h in culture, the cells in the second set of wells were re-suspended, stained with 100 ng/ml PI, and cell viability determined by flow cytometry. Columns show mean ± S.E.M., where $n = 3$ independently performed experiments

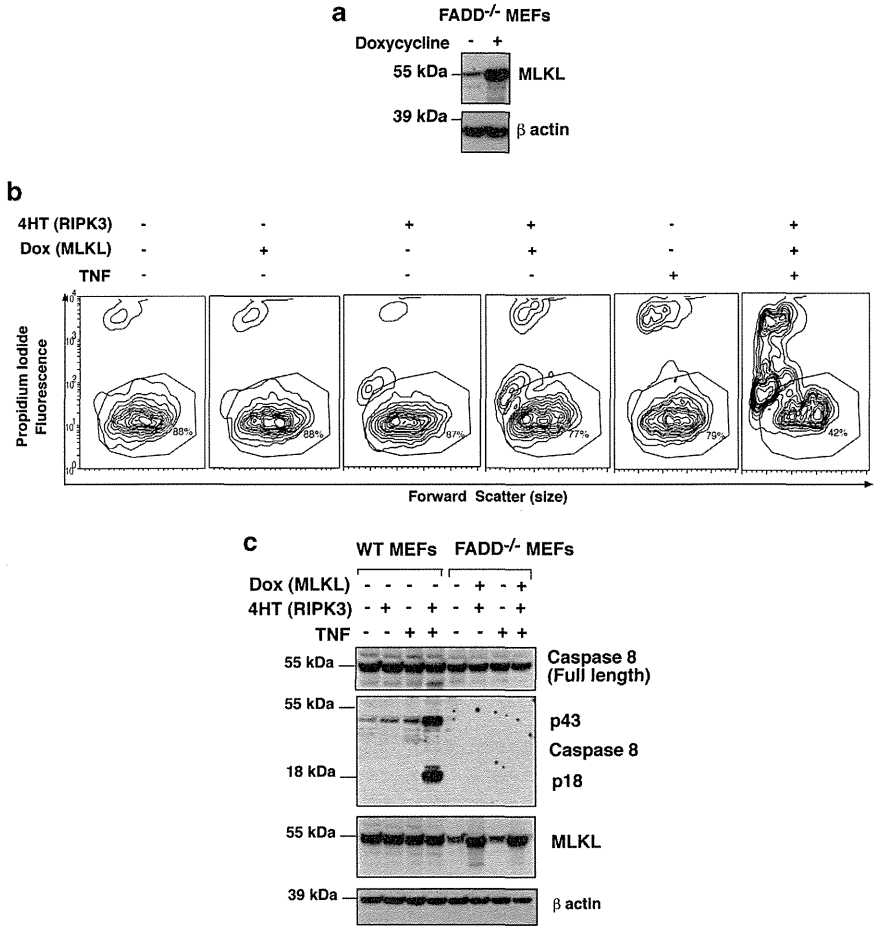

Figure 6 Elevated levels of MLKL in *Fadd*$^{-/-}$ MEFs allows cell death by TNF-induced activation of RIPK3. (**a**) *Fadd*$^{-/-}$ MEFs were infected with a doxycycline (dox)-inducible MLKL expression vector. Cells were treated with 1 μg/ml of dox for 24 h. Cell lysates were harvested and probed for MLKL as indicated and β-actin was used as a loading control. (**b**) *Fadd*$^{-/-}$ MEFs bearing vectors for dox-inducible MLKL and 4HT-inducible RIPK3 were treated with 1 μg/ml dox, 10 nM 4HT, and 100 ng/ml TNF for 24 h. Cells were re-suspended using trypsin, stained with 100 ng/ml PI, and analyzed by flow cytometry. (**c**) WT MEFs bearing a 4HT-inducible RIPK3 vector and *Fadd*$^{-/-}$ MEFs bearing vectors for 4HT-inducible RIPK3 and dox-inducible MLKL were treated with 1 μg/ml dox and 10 nM 4HT for 24 h and treated with 100 ng/ml TNF for 4 h. Cell lysates were harvested and probed for caspase 8 (full-length), cleaved caspase 8 and MLKL as indicated, and β-actin was used as a loading control

levels of MLKL, and when MLKL levels were elevated, TNF was able to kill the *Fadd*$^{-/-}$ cells. These results suggest that FADD might be needed for activation of caspase 8, but is not required for TNFR1 to activate RIPK3 and MLKL to cause necroptosis.

The necroptotic cell death pathway triggered by TNF in cells with elevated RIPK3 did not require the presence of FADD, RIPK1, caspase 8, or Bax/Bak. The ability of induced MLKL to restore the sensitivity of the *Fadd*$^{-/-}$ cells is consistent with MLKL being activated by RIPK3 and having an important role in necroptosis.[22] Although how MLKL kills has not yet been determined with certainty, our observations are consistent with reports that it causes cell death by a caspase- and Bax/Bak-independent mechanism.[17,22]

Our results are consistent with the model shown in Figure 7. WT MEFs remain viable when TNF is added, because cIAP1, TRAF2, and RIPK1 allow activation of canonical NF-κB pathways resulting in the expression of cell death inhibitors such as FLIP, cIAP2, and A20[28,36,37] (panel 1). When smac-mimetic is added, it causes autoubiquitylation and degradation of IAPs, so that cells treated with TNF plus smac-mimetic die by a caspase 8- and RIPK1-dependent mechanism (panel 2).

When levels of RIPK3 are elevated (panel 3), ligation of TNFR1 signals via TRADD to activate RIPK3, and TNF can trigger RIPK3 activation even when RIPK1 is absent. Once activated, RIPK3 can in turn activate two distinct cell death pathways, one involving caspase 8, and another that involves MLKL (panel 3). In *Fadd*$^{-/-}$ MEFs, ligation of TNFR1 can activate RIPK3 when its levels are elevated, and it can activate the necroptotic pathway but not the caspase 8-dependent cell death pathway (panel 4).

These findings do not exclude the possibility that RIPK1 can activate RIPK3; indeed, this is likely to be what occurs when necrostatin is able to inhibit cell death.[11,19] These findings are also consistent with a model in which RIPK1 acts in parallel with RIPK3 such that in the presence of RIPK1, lower levels of RIPK3 are needed for necroptosis. However, our results provide strong evidence that RIPK1 does not have an obligatory role in necroptosis signaling, challenging models

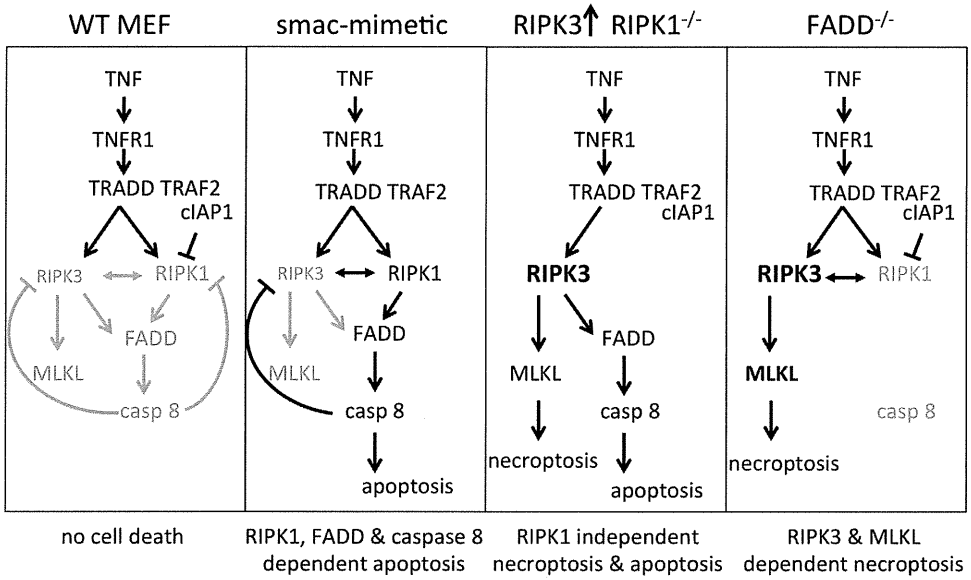

Figure 7 Model for activation of caspase-dependent and -independent cell death mechanisms by TNF. Under normal conditions, TNF treatment of WT MEFs does not induce cell death. When IAPs are depleted with smac-mimetic, TNF can activate caspase 8 by a pathway requiring RIPK1 to cause cell death that can be blocked by the caspase inhibitor Q-VD-OPh. When levels of RIPK3 are elevated, TNF not only activates caspase 8 but also activates a caspase-independent death mechanism, but it does not require RIPK1 for either

which suggested that RIPK1 has an essential role upstream of RIPK3 and is required for its activation.

Materials and Methods

Genetically modified cell lines and mice. Production of MEF lines has been described previously in detail.[7] Briefly, primary MEFs were generated from E15.5 embryos and then infected with SV40 large T antigen-expressing lentivirus to generate immortal cell lines. *Ripk1*$^{-/-}$ mice were provided by Michelle Kelliher (University of Massachusetts Medical School, Worcester, MA, USA) and *Tnfr1*$^{-/-}$ and *Tnfr2*$^{-/-}$ mice were a kind gift from Heinrich Korner (University of Tasmania, Sandy Bay, TAS, Australia). *Fadd*$^{-/-}$ MEFs were provided by Francis Chan (University of Massachusetts Medical School), *Tradd*$^{-/-}$ MEFs were obtained from Henning Walczak (Imperial College, London, UK) and Manolis Pasparakis (University of Cologne, Cologne, Germany), and *Bax/Bak*$^{-/-}$ MEFs were provided by David Huang (Walter and Eliza Hall Institute, Parkville, VIC, Australia). Caspase 8 conditional knockin mice were provided by Stephen Hedrick (University of California San Diego, San Diego, CA, USA).

Generation of *caspase 8*$^{-/-}$ MEFs. Caspase 8 gene-deleted MEFs were generated from E8.5 caspase 8 LoxP/LoxP embryos (Dr. Steve Hedrick, University of California San Diego). Primary MEFs were immortalized by infection with SV40 largeT antigen-expressing lentivirus as described previously.[7] To delete caspase 8, the transformed MEFs were infected with a Cre-recombinase-expressing lentivirus (pFU CreR SV40 Hygro) and deletion was confirmed by western blot.

Cell culture, transfections, constructs and lentiviral infections. Cell lines were maintained at 37° C, 10% CO_2 in DMEM supplemented with 10% (v/v) fetal bovine serum (Gibco, Melbourne, VIC, Australia), 50 μg/ml penicillin G, 50 U/ml streptomycin, and 2 mM L-glutamine. Medium for *Bax/Bak*$^{-/-}$ MEFs was also supplemented with 270 μM L-asparagine and 50 μM 2-mercaptoethanol. Cre-recombinase and SV40 large T antigen were cloned into the lentiviral vector pFU as described previously.[7] Mouse FLAG-RIPK3 was cloned into the 4HT-inducible lentiviral vector pF 5 × UAS.[7,38] Lentiviruses were generated by transfecting subconfluent 10 cm plates of 293T cells with vector plasmids together with the packaging constructs pCMV-ΔR8 and pVSV-G using Effectene (Qiagen, Chadstone, VIC, Australia) as described previously.[38] After 48 h, viral supernatants were collected, filtered, supplemented with 4 μg/ml polybrene, and added to the target MEFs. Stably infected cells were selected in the presence of 5 μg/ml puromycin (puro) and 300 μg/ml hygromycin B. Expression of pF 5 × UAS-inducible constructs was induced with 10 nM 4HT, unless otherwise indicated. The doxycycline-inducible vector pF TRE3G PGK puro is a derivative of the pRetroX retroviral vector (Clontech, Mountain View, CA, USA) possessing a Tet-On 3G transactivator (Tet3G), a puro resistance gene expressed under the control of a PGK promoter, and a tetracycline-responsive element.[39] The cDNA-encoding mouse MLKL (residues 1–464; UniProt sequence Q9D2Y4-2) was PCR amplified using the following primers: forward, 5′-CGCGGATCCAAGCCACCATGGCGCGC CAGGAC-3′; reverse, 5′-CGCGGATCCTTACACCTTCTTGTCCGTGGATTC-3′. The *Bam*HI-digested PCR product was ligated into the *Bam*HI site of the pF TRE3G PGK puro vector and was verified by sequencing (Micromon DNA Sequencing Facility, Clayton, VIC, Australia).

Antibodies and chemicals. Primary antibodies used for western blot analysis were anti-FLAG (F-3165; Sigma, Croydon, VIC, Australia), anti-β-actin (A-1978; Sigma), anti-RIPK1 (610458; BD Transduction Laboratories, North Ryde, NSW, Australia), anti-RIPK3 (551042; Pharmingen, North Ryde, NSW, Australia), anticaspase 8 (Lorraine O'Reilly, The Walter and Eliza Hall Institute, Melbourne, VIC, Australia), anticleaved caspase 8 (Asp 387) (8592; Cell Signaling Technology, Arundel, QLD, Australia), anticleaved caspase 3 (Asp 175) (9661; Cell Signaling Technology), anti-PARP (9542; Cell Signaling Technology, Arundel, Queensland Australia), and anti-MLKL (Jian-Guo Zhang, The Walter and Eliza Hall Institute). 4HT and doxycycline were purchased from Sigma, Fc-TNF (in-house) and Q-VD-OPh (OPH001) from SM Biochemicals, (Anaheim, CA, USA) and smac-mimetic was obtained from TetraLogic Pharmaceuticals (Malvern, PA, USA).

Cell death assays. Cells were seeded at approximately 40% confluency onto 12-well tissue culture plates and were allowed to settle for 16–20 h. Where indicated, 500 nM smac-mimetic (Compound A; TetraLogic Pharmaceuticals), 100 ng/ml human Fc-TNF, 10 nM 4HT, and/or 10 μM Q-VD-OPh were added to cells for 24 h and cell death measured by uptake of propidium iodide (PI) using a FACScalibur flow cytometer (BD Biosciences, North Ryde, NSW, Australia). In all, 10 000 events per sample were collected, and the percentage of live cells (% PI-negative cells) was quantified using WEASEL software (version 2.2.2; WEHI).

Clonogenic survival assay. WT, *caspase 8*$^{-/-}$, *Ripk1*$^{-/-}$, and *Bax/Bak*$^{-/-}$ MEFs were plated at equal densities on six-well plates, and cultured with or without TNF and smac-mimetic for 24 h. After treatment, cells were treated with trypsin, re-suspended, washed, and re-plated. Cells were then grown

for 5 days and fixed with glutaraldehyde, and colonies stained with 0.1% (w/v) crystal violet.

Western blotting. Lysates were prepared in DISC lysis buffer (20 mM Tris-HCl (pH 7.4), 150 mM NaCl, 10% glycerol, 10% Triton X-100), supplemented with protease inhibitor cocktail (Roche, Dee Why,NSW Australia). Protein samples were separated on 4–12% polyacrylamide gels (Invitrogen, Mulgrave, VIC, Australia), and transferred to Hybond C nitrocellulose membrane (GE, Rydalmere, NSW, Australia) for incubation with specified antibodies. All membrane blocking steps and antibody dilutions were performed using 5% (v/v) skim milk in PBS containing 0.1% (v/v) Tween-20 phosphate-buffered saline (PBST), and washing steps performed with PBST. Western blots were visualized by enhanced chemiluminescence (GE).

Conflict of Interest

The authors declare no conflict of interest.

Acknowledgements. This work was funded by NHMRC grants and fellowships 433063, 461221, 541901, 575512, 637342, 1003435, and ARC fellowship FT100100100, and was made possible through Victorian State Government Operational Infrastructure Support and Australian Government NHMRC IRIISS. We thank Stephen Hedrick, Michelle Kelliher, and Heinrich Korner for caspase 8, TRADD, FADD, and RIPK1 gene-deleted cell lines and mice, and Mark McKinlay (TetraLogic Pharmaceuticals) for smac-mimetic compound. We would also like to acknowledge Ian Gentle for helping construct the 4HT-inducible FLAG RIPK3 construct.

1. Baud V, Karin M. Signal transduction by tumor necrosis factor and its relatives. *Trends Cell Biol* 2001; **11**: 372–377.
2. Laster SM, Wood JG, Gooding LR. Tumor necrosis factor can induce both apoptic and necrotic forms of cell lysis. *J Immunol* 1988; **141**: 2629–2634.
3. Beg AA, Baltimore D. An essential role for Nf-Kappa-B in preventing Tnf-alpha-induced cell death. *Science* 1996; **274**: 782–784.
4. Chinnaiyan AM, Tepper CG, Seldin MF, Orourke K, Kischkel FC, Hellbardt S *et al.* Fadd/mort1 is a common mediator of cd95 (fas/apo-1) and tumor necrosis factor receptor-induced apoptosis. *J Biol Chem* 1996; **271**: 4961–4965.
5. Varfolomeev EE, Boldin MP, Goncharov TM, Wallach D. A potential mechanism of cross-talk between the p55 tumor necrosis factor receptor and fas/apo1 – proteins binding to the death domains of the two receptors also bind to each other. *J Exp Med* 1996; **183**: 1271–1275.
6. Muzio M, Stockwell BR, Stennicke HR, Salvesen GS, Dixit VM. An induced proximity model for caspase-8 activation. *J Biol Chem* 1998; **273**: 2926–2930.
7. Vince JE, Wong WW, Khan N, Feltham R, Chau D, Ahmed AU *et al.* IAP antagonists target cIAP1 to induce TNFalpha-dependent apoptosis. *Cell* 2007; **131**: 682–693.
8. Zhou Q, Snipas S, Orth K, Muzio M, Dixit VM, Salvesen GS. Target protease specificity of the viral serpin crma – analysis of five caspases. *J Biol Chem* 1997; **272**: 7797–7800.
9. Caserta TM, Smith AN, Gultice AD, Reedy MA, Brown TL. Q-VD-OPh a broad spectrum caspase inhibitor with potent antiapoptotic properties. *Apoptosis* 2003; **8**: 345–352.
10. Kunstle G, Leist M, Uhlig S, Revesz L, Feifel R, Mackenzie A *et al.* Ice-protease inhibitors block murine liver injury and apoptosis caused by cd95 or by tnf-alpha. *Immunol Lett* 1997; **55**: 5–10.
11. Degterev A, Huang Z, Boyce M, Li Y, Jagtap P, Mizushima N *et al.* Chemical inhibitor of nonapoptotic cell death with therapeutic potential for ischemic brain in jury. *Nat Chem Biol* 2005; **1**: 112–119.
12. Vercammen D, Beyaert R, Denecker G, Goossens V, Van Loo G, Declercq W *et al.* Inhibition of caspases increases the sensitivity of L929 cells to necrosis mediated by tumor necrosis factor. *J Exp Med* 1998; **187**: 1477–1485.
13. Declercq W, Vanden Berghe T, Vandenabeele P. RIP kinases at the crossroads of cell death and survival. *Cell* 2009; **138**: 229–232.
14. Cho YS, Challa S, Moquin D, Genga R, Ray TD, Guildford M *et al.* Phosphorylation-driven assembly of the RIP1–RIP3 complex regulates programmed necrosis and virus-induced inflammation. *Cell* 2009; **137**: 1112–1123.
15. Feoktistova M, Geserick P, Kellert B, Dimitrova DP, Langlais C, Hupe M *et al.* cIAPs block ripoptosome formation, a RIP1/caspase-8 containing intracellular cell death complex differentially regulated by cFLIP isoforms. *Mol Cell* 2011; **43**: 449–463.
16. Tenev T, Bianchi K, Darding M, Broemer M, Langlais C, Wallberg F *et al.* The ripoptosome, a signaling platform that assembles in response to genotoxic stress and loss of IAPs. *Mol Cell* 2011; **43**: 432–448.
17. Wang Z, Jiang H, Chen S, Du F, Wang X. The mitochondrial phosphatase PGAM5 functions at the convergence point of multiple necrotic death pathways. *Cell* 2012; **148**: 228–243.
18. Zhang DW, Shao J, Lin J, Zhang N, Lu BJ, Lin SC *et al.* RIP3, an energy metabolism regulator that switches TNF-induced cell death from apoptosis to necrosis. *Science* 2009; **325**: 332–336.
19. Degterev A, Hitomi J, Germscheid M, Ch'en IL, Korkina O, Teng X *et al.* Identification of RIP1 kinase as a specific cellular target of necrostatins. *Nat Chem Biol* 2008; **4**: 313–321.
20. Sun X, Lee J, Navas T, Baldwin DT, Stewart TA, Dixit VM. RIP3 a novel apoptosis-inducing kinase. *J Biol Chem* 1999; **274**: 16871–16875.
21. Micheau O, Tschopp J. Induction of TNF receptor I-mediated apoptosis via two sequential signaling complexes. *Cell* 2003; **114**: 181–190.
22. Sun L, Wang H, Wang Z, He S, Chen S, Liao D *et al.* Mixed lineage kinase domain-like protein mediates necrosis signaling downstream of RIP3 kinase. *Cell* 2012; **148**: 213–227.
23. Vanlangenakker N, Vanden Berghe T, Bogaert P, Laukens B, Zobel K, Deshayes K *et al.* cIAP1 and TAK1 protect cells from TNF-induced necrosis by preventing RIP1/RIP3-dependent reactive oxygen species production. *Cell Death Differ* 2011; **18**: 656–665.
24. He S, Wang L, Miao L, Wang T, Du F, Zhao L *et al.* Receptor interacting protein kinase-3 determines cellular necrotic response to TNF-alpha. *Cell* 2009; **137**: 1100–1111.
25. Kaiser WJ, Offermann MK. Apoptosis induced by the toll-like receptor adaptor TRIF is dependent on its receptor interacting protein homotypic interaction motif. *J Immunol* 2005; **174**: 4942–4952.
26. Li J, McQuade T, Siemer AB, Napetschnig J, Moriwaki K, Hsiao YS *et al.* The RIP1/RIP3 necrosome forms a functional amyloid signaling complex required for programmed necrosis. *Cell* 2012; **150**: 339–350.
27. Vandenabeele P, Declercq W, Van Herreweghe F, Vanden Berghe T. The role of the kinases RIP1 and RIP3 in TNF-induced necrosis. *Sci Signal* 2010; **3**: 4.
28. Moujalled DM, Cook WD, Lluis JM, Khan NR, Ahmed AU, Callus BA *et al.* In mouse embryonic fibroblasts, neither caspase-8 nor cellular FLICE-inhibitory protein (FLIP) is necessary for TNF to activate NF-kappaB, but caspase-8 is required for TNF to cause cell death, and induction of FLIP by NF-kappaB is required to prevent it. *Cell Death Differ* 2011; **5**: 808–815.
29. Wong WW, Gentle IE, Nachbur U, Anderton H, Vaux DL, Silke J. RIPK1 is not essential for TNFR1-induced activation of NF-kappaB. *Cell Death Differ* 2009; **3**: 482–487.
30. Abhari BA, Cristofanon S, Kappler R, von Schweinitz D, Humphreys R, Fulda S. RIP1 is required for IAP inhibitor-mediated sensitization for TRAIL-induced apoptosis via a RIP1/FADD/caspase-8 cell death complex. *Oncogene* 2012; e-pub ahead of print, 13 August 2012; doi:10.1038/onc.2012.337.
31. Upton JW, Kaiser WJ, Mocarski ES. DAI/ZBP1/DLM-1 complexes with RIP3 to mediate virus-induced programmed necrosis that is targeted by murine cytomegalovirus vIRA. *Cell Host Microbe* 2012; **11**: 290–297.
32. Irrinki KM, Mallilankaraman K, Thapa RJ, Chandramoorthy HC, Smith FJ, Jog NR *et al.* Requirement of FADD, NEMO, and BAX/BAK for aberrant mitochondrial function in tumor necrosis factor alpha-induced necrosis. *Mol Cell Biol* 2011; **31**: 3745–3758.
33. Zhao J, Jitkaew S, Cai Z, Choksi S, Li Q, Luo J *et al.* Mixed lineage kinase domain-like is a key receptor interacting protein 3 downstream component of TNF-induced necrosis. *Proc Natl Acad Sci USA* 2012; **109**: 5322–5327.
34. Gentle IE, Wong WW, Evans JM, Bankovacki A, Cook WD, Khan NR *et al.* In TNF-stimulated cells, RIPK1 promotes cell survival by stabilizing TRAF2 and cIAP1, which limits induction of non-canonical NF-kappaB and activation of caspase-8. *J Biol Chem* 2011; **286**: 13282–13291.
35. Yu PW, Huang BC, Shen M, Quast J, Chan E, Xu X *et al.* Identification of RIP3, a RIP-like kinase that activates apoptosis and NFkappaB. *Curr Biol* 1999; **9**: 539–542.
36. Chu ZL, Mckinsey TA, Liu L, Gentry JJ, Malim MH, Ballard DW. Suppression of tumor necrosis factor-induced cell death by inhibitor of apoptosis c-iap2 is under nf-kappa-b control. *Proc Natl Acad Sci USA* 1997; **94**: 10057–10062.
37. He KL, Ting AT. A20 inhibits tumor necrosis factor (TNF) alpha-induced apoptosis by disrupting recruitment of TRADD and RIP to the TNF receptor I complex in Jurkat T cells. *Mol Cell Biol* 2002; **22**: 6034–6045.
38. Callus BA, Moujallad DM, Silke J, Gerl R, Jabbour AM, Ekert PG *et al.* Triggering of apoptosis by Puma is determined by the threshold set by prosurvival Bcl-2 family proteins. *J Mol Biol* 2008; **384**: 313–323.
39. Yamamoto M, Okuyama M, Ma JS, Kimura T, Kamiyama N, Saiga H *et al.* A cluster of interferon-gamma-inducible p65 GTPases plays a critical role in host defense against *Toxoplasma gondii*. *Immunity* 2012; **37**: 302–313.

Supplementary Information accompanies the paper on Cell Death and Disease website (http://www.nature.com/cddis)

ACS chemical biology

Letters

pubs.acs.org/acschemicalbiology

Stabilizing the Pro-Apoptotic BimBH3 Helix (BimSAHB) Does Not Necessarily Enhance Affinity or Biological Activity

Toru Okamoto,[†,‡] Kerry Zobel,[§] Anna Fedorova,[§] Clifford Quan,[§] Hong Yang,[†,‡] Wayne J. Fairbrother,[§] David C. S. Huang,[†,‡] Brian J. Smith,[*,†,‡,∥] Kurt Deshayes,[*,§] and Peter E. Czabotar[*,†,‡]

[†]The Walter and Eliza Hall Institute of Medical Research, 1G Royal Parade, Parkville, Victoria 3052, Australia

[‡]Department of Medical Biology, University of Melbourne, Parkville, Victoria 3010, Australia

[§]Departments of Early Discovery Biochemistry and Protein Engineering, Genentech Inc., 1 DNA Way, South San Francisco, California 94080, United States

[∥]Department of Chemistry, La Trobe Institute for Molecular Sciences, La Trobe University, Melbourne, Victoria 3086, Australia

S *Supporting Information*

ABSTRACT: An attractive approach for developing therapeutic peptides is to enhance binding to their targets by stabilizing their α-helical conformation, for example, stabilized BimBH3 peptides (BimSAHB) designed to induce apoptosis. Unexpectedly, we found that such modified peptides have *reduced* affinity for their targets, the pro-survival Bcl-2 proteins. We attribute this loss in affinity to disruption of a network of stabilizing intramolecular interactions present in the bound state of the native peptide. Altering this network may compromise binding affinity, as in the case of the BimBH3 stapled peptide studied here. Moreover, cells exposed to these peptides do not readily undergo apoptosis, strongly indicating that BimSAHB is not inherently cell permeable.

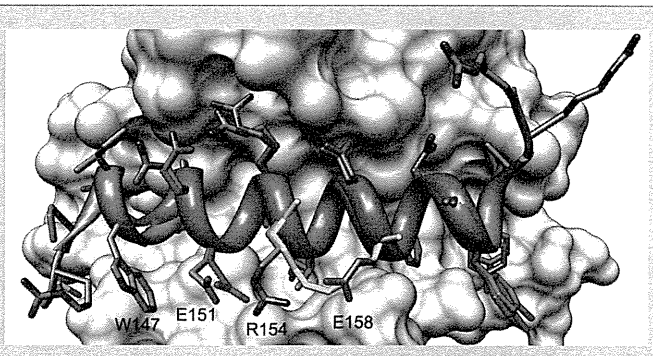

Stabilized helical peptides are designed to mimic an α-helical structure through a constraint imposed by covalently linking two residues on the same helical face (e.g., residue *i* with *i* + 4). "Stapling" the peptide into a preformed helix might be expected to lower the energy barrier for binding by reducing entropic costs, with a concomitant increase in binding affinity. Additionally, stabilizing the peptide may reduce degradation by proteases[1,2] and, in the case of hydrocarbon linkages, reportedly enhance transport into cells,[3] thereby improving bioavailability and their potential as therapeutic agents.[3−5] The findings we present here for the stapled BH3 peptide (BimSAHB), however, do not support these claims, particularly in regards to affinity and cell permeability. We observe a reduction in binding upon BimBH3 stapling, which we attribute to the loss of a network of stabilizing intramolecular interactions on the peptide. Thus, in addition to the primary consideration for staple placement in peptide design, that of avoiding key binding interfaces, our observations reveal a new consideration, that staples should also avoid disruption of favorable interactions within the peptide itself.

It has previously been reported that a stapled version of the BimBH3 peptide (dubbed: "stabilized α-helices of Bcl-2 domains", BimSAHB), where two native residues were replaced with (*S*)-pentenyl alanine derivatives and covalently joined through a metathesis reaction,[2,3] kills cells by directly activating Bax through an interface involving residue Lys21.[6] This stabilized peptide has also been reported to have enhanced binding for the pro-survival proteins.[7] When mouse embryonic fibroblasts (MEFs) (Supplementary Figure 1) or Jurkat cells (data not shown) were treated with BimSAHB, we observed no cell death, in contrast to the potent killing induced by the well-characterized activator of apoptosis, etoposide. This was true for both the 20-mer BimSAHB peptide used below and the 21-mer BimSAHB peptide previously used in cellular assays.[8]

Given that no cell killing was observed when BimSAHB was added to cells in culture, we decided to test the ability of these peptides to induce mitochondrial cytochrome *c* release *in vitro* from cells permeabilized with a low concentration of the detergent digitonin. This would determine if the absence of killing activity could be attributed to a lack of cellular uptake. In such assays, we found that BimSAHB was indeed capable of liberating mitochondrial cytochrome *c* (Figure 1a,b), consistent with the conclusion that BimSAHB, under the conditions tested, does not readily enter cells in sufficient amounts to induce apoptosis (although proteolytic degradation or non-specific binding effects could also account for this observation).

We next tested the role of the Bax interface encompassing Lys21 proposed to be essential for its activation.[6] To undertake

Received: October 18, 2011
Accepted: November 14, 2012

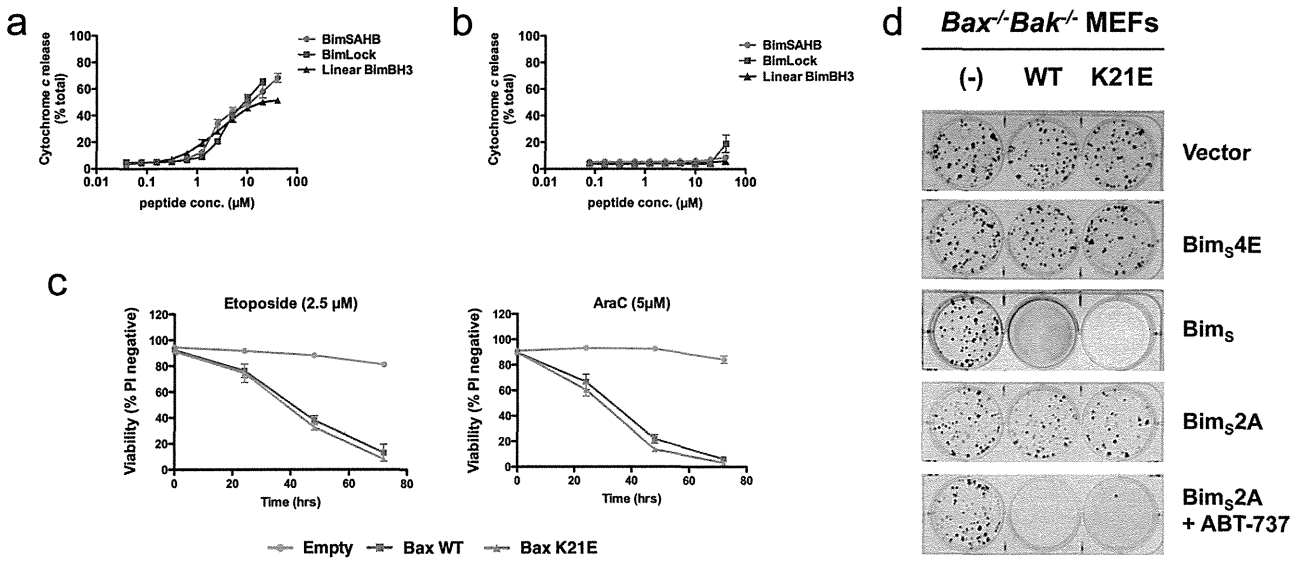

Figure 1. Bioactivity of constrained BimBH3 peptides. Cytochrome *c* release experiments were performed on permeabilized cells (MEFs) that were derived from either (a) wild-type or (b) from $Bax^{-/-}Bak^{-/-}$ mice. The cell pellets, containing intact mitochondria, were treated with increasing concentrations of the indicated peptides. The quantity of cytochrome *c* release was assessed by ELISA (R&D Systems) analyses of supernatants postpeptide treatment as compared to mitochondria treated with the permeabilizing agent 1% Triton X-100 (100% activity). (c) Killing assay of $Bax^{-/-}Bak^{-/-}$ MEF cells reconstituted with either wild-type Bax (WT) or Bax(K21E) in response to DNA damaging agents etoposide or Ara-C. Cell viability was monitored by propidium iodide (PI) exclusion determined by flow cytometry. Expression of wild-type Bax and BaxK21E were confirmed by Western blot analysis (Supplementary Figure 2). (d) Colony formation assays of $Bax^{-/-}Bak^{-/-}$ MEF cells reconstituted with either wild-type Bax (WT) or Bax (K21E) and transfected with vector encoding an inactive Bim variant (Bim_S4E),[20] wild-type Bim_S (targeting all pro-survival proteins), a Bim_S variant targeting only Mcl-1 (Bim_S2A),[21] or Bim_S2A in combination with ABT-737 treatment. Error bars in panels a–c represent SEM of 2 independent experiments.

this, we reconstituted MEFs lacking the essential cell death mediators Bax and Bak with wild-type (WT) Bax or the K21E mutant that was reported to be inert.[6] Unexpectedly, cells reconstituted with either WT or K21E mutant Bax behaved identically in short- or long-term survival assays (Figure 1c,d), suggesting that this interface was not required for Bax activation. Equivalent cell death to that observed for BimBH3 overexpression was observed when ABT-737 (to target Bcl-2, Bcl-x_L, and Bcl-w[7]) was combined with Bim_S2A (to target Mcl-1[9]), suggesting that apoptosis in these cells is primarily the result of inhibition of pro-survival proteins (Figure 1d).[10] By implication, the mechanism by which BimBH3 peptides initiate cytochrome *c* release in our experiments using isolated mitochondria could be accounted for by relieving the pro-survival proteins restraining Bax and Bak[10] and possibly by direct activation of Bax via an alternative interface such as that shown for Bak.[11]

In sharp contrast to the reported studies,[3] our studies suggest that BimSAHB is not inherently cell permeable. Moreover, the linear control BimBH3 of precisely the same length as the stapled peptide was just as active at inducing cytochrome *c* release *in vitro* (Figure 1a). As the proposed interface for Bax activation by BimSAHB did not appear to play a major role (Figure 1c,d), we undertook a detailed biochemical and structural analysis of the constrained BimSAHB and its interactions with pro-survival proteins. To undertake these studies, we also employed a second approach, which we termed BimLOCK, to link the side-chains of a glutamate with a lysine through a lactam bridge.[12,13] These modified residues were identical to the (*S*)-pentenyl alanines used to construct BimSAHB.

Circular dichroism (CD) was employed to confirm that covalent linkages enhanced helical content (Figure 2a). Both BimSAHB (39% helix) and BimLOCK (49%) displayed enhanced helical content in an aqueous solution compared to an equivalent linear peptide (21%). Additionally, we determined crystal structures for both constrained peptides in complex with the pro-survival Bcl-2 family protein Bcl-x_L (BCL2L1) (Figure 2b,c). These structures revealed that both constrained peptides bind to Bcl-x_L analogously to the linear BimBH3 peptide and that neither the hydrocarbon staple nor the lactam bridge interacts with residues on Bcl-x_L. Because of the increased helicity, we anticipated an approximate 4-fold increase in binding affinity (see Supporting Information). Instead, these peptides have reduced affinities for pro-survival proteins (Table 1a). Direct binding assays confirmed this observation for two pro-survival proteins, Bcl-x_L and Mcl-1. The penalty imposed by the staple for Bcl-x_L is due to slower on- and faster off-rates (1.8- and 13-fold, respectively). Similarly, the loss in affinity for Mcl-1 resulted predominantly from a faster off-rate (2.8-fold increase, compared to a 1.3-fold reduction in on-rate) (Table 1b).

Inspection of the structure of BimBH3-peptide in complex with Bcl-x_L (PDB code, 3FDL[14]) reveals how the side-chain groups of residues on the exposed face of the peptide form a series of interactions with one another; Glu151 and Glu158 (numbering based on human Bim_{EL}) form a pair of salt bridges with Arg154, and the aliphatic methylene moiety of Glu151 packs tightly with the indole side-chain of Trp147. Additionally, Arg154 of Bim forms a water-mediated interaction with Arg103 of Bcl-x_L (Supplementary Figure 3a). Critically, none of these interactions are observed in either structure of the stapled peptides in complex with Bcl-x_L (Supplementary Figure 3b,c).

We have calculated the pairwise interaction energy between the side-chain groups of each of these residues employing the AUTODOCK empirical function: the AUTODOCK potential

dx.doi.org/10.1021/cb3005403 | *ACS Chem. Biol.* XXXX, XXX, XXX–XXX

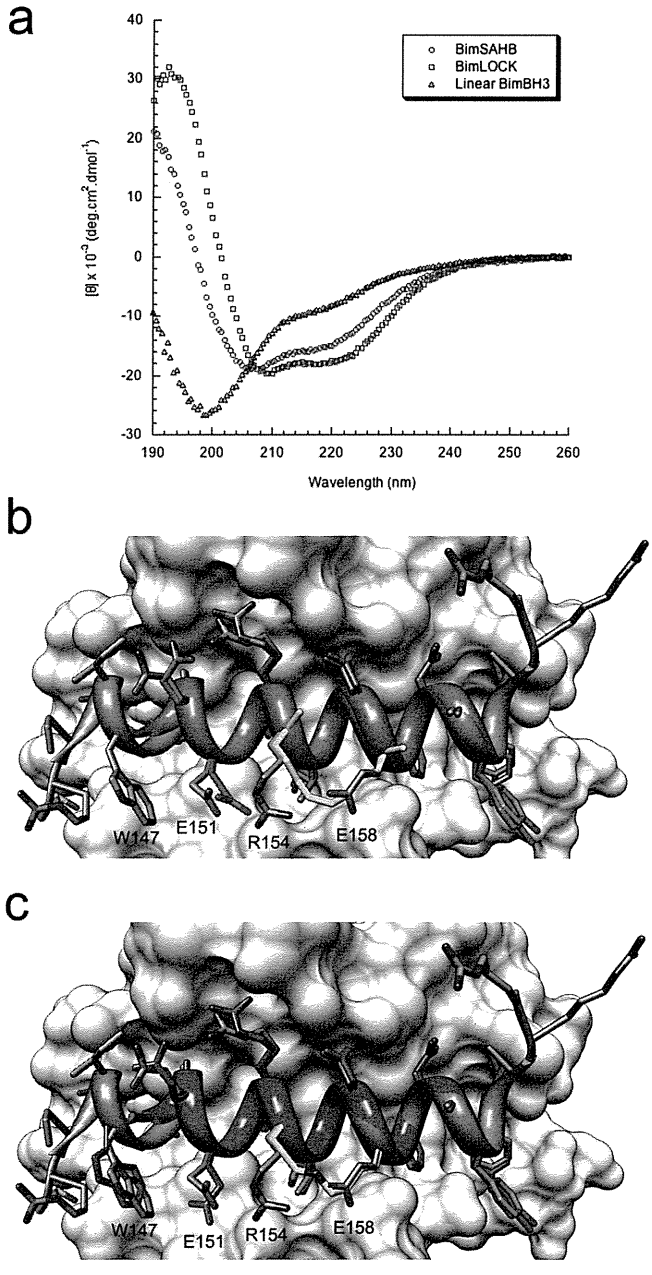

Figure 2. Characterization of constrained BimBH3 peptides. (a) Circular dichroism was used to measure the percentage of helical content for BimSAHB, BimLOCK, and an equivalent linear BimBH3 peptide. Both constrained BimBH3 peptides were found to have significant helical content (BimSAHB 39% helix; BimLOCK 49% helix), while the linear peptide was found to have a modest secondary structure content (21% helix). (b) Structure of the Bcl-x_L:BimSAHB complex overlaid with linear BimBH3 peptide in complex with Bcl-x_L (PDB code, 3FDL;[14] note that the peptide used for the 3FDL structure is longer than those used in this study). Peptide regions of BimSAHB are colored green and the hydrocarbon staple yellow. (c) Structure of the Bcl-x_L:BimLOCK complex overlaid with BimBH3. Peptide regions of BimLOCK are colored magenta and the lactam bridge yellow. BimBH3 is colored blue, and Bcl-x_L is represented in surface format in both complexes. Peptide sequences are as detailed in Table 1 unless otherwise stated.

includes five major contributions to the total free energy of interaction: the van der Waals, hydrogen-bond, electrostatic, conformational entropy, and desolvation energies.[15] The individual energies of interaction calculated were, between Trp147–Glu151, −0.3 kJ mol^{-1}, Glu151–Arg154, −7.0 kJ mol^{-1}, and Arg154–Glu158, −2.7 kJ mol^{-1} (using the Bcl-x_L/Bim coordinates), yielding a total interaction energy between all four residues of −10.0 kJ mol^{-1}. Assuming these side-chains do not interact with one another in the free peptide, the cumulative effect of increased helicity of the peptide and estimated loss in binding energy due to missing side-chain interactions, the anticipated reduction in binding affinity for BimSAHB and BimLOCK is 24-fold and 16-fold, respectively. These estimates compare favorably with the observed 26-fold reduction from the competition assay and 8-fold reduction from the direct binding assay for BimSAHB (Table 1, Supplementary Table 2) and, likewise, 3-fold reduction from the competition assay for BimLOCK.

For Mcl-1 and A1, where the reduction in binding affinity observed by the introduction of the constraint is not as large as that observed for Bcl-2 and Bcl-x_L, either the side-chain groups may maintain some interaction with one another or the side-chain groups may interact with the pro-survival receptor to improve binding affinity. To further assess the contribution of the intramolecular bonding network on the exposed face of the peptide and to ensure loss of affinity could not be attributed to steric hindrance imposed by the staple, we tested the binding affinity of an unstapled Bim peptide (linear Bim with Glu151 and Arg154 substituted with pentenylalanine residues but not subjected to ring closing metathesis) (Table 1b). This peptide bound Bcl-x_L with a further reduced affinity as compared to the stapled Bim, as would be anticipated with the combined effects of a reduction in helicity (due to loss of the staple) and the loss of the stabilizing intramolecular network.

Upon binding their pro-survival receptor, the BH3 peptides adopt an α-helical geometry, stabilized by the interactions between receptor and peptide *and* by the intramolecular interactions within the peptide, specifically the classical hydrogen bond between the carbonyl oxygen and the NH groups (i with $i + 4$) and also the interactions between the side-chain groups. Disrupting the latter of these interactions results in a decrease in binding affinity; in our estimate, this is ~10 kJ mol^{-1} in the case of the BimBH3 peptide. The introduction of the staple into the peptides has two consequences: (i) while the staple is able to preorganize the helix and reduce the entropic penalty for the association, the introduction of a covalent bond between side-chains removes the contribution to the binding energy that comes about when the two residues interact (in the salt bridge formed between Arg154 and Glu158, we estimate this to be 2.7 kJ mol^{-1}), and (ii) the chemical nature of the staple may not be conducive to forming stable interactions with the side-chain group of the residue one turn away. Loss of a stable interaction with the staple can be perpetuated down the chain; in both stapled peptides here, the result is the loss of all stabilizing interactions between side-chains, most critically the loss of the salt-bridge between Glu151 and Arg154. The binding free energy reflects the change in free energy between unbound and bound states, and since the covalent linkage is present in both states, there is no change in free energy of interaction across the staple upon binding. In contrast, in the native peptide, we calculate a significant favorable change in intramolecular energy of the ligand upon binding.

The structures of the peptides in complex with pro-survival Bcl-x_L reveal that they bind analogously to unrestrained BimBH3, neither modification interacting directly with the target protein unlike that observed with another stabilized peptide in complex with Mcl-1[16] where the staple itself makes

dx.doi.org/10.1021/cb3005403 | ACS Chem. Biol. XXXX, XXX, XXX–XXX

Table 1. Analyses of Binding of BimBH3 Peptides to Pro-Survival Proteins Using Biacore-Based Assays

a					
K_i (nM)	Bcl-2	Bcl-x_L	Bcl-w	Mcl-1	A1
BimSAHB	460 ± 80	300 ± 37	370 ± 61	3.4 ± 0.1	4.1 ± 0.3
BimLOCK	800 ± 27	35 ± 3.7	37 ± 3.0	3.7 ± 0.3	4.7 ± 0.1
Linear Bim	6.8 ± 1.6	11 ± 0.6	25 ± 2.3	<1.4	<2.5

b	on-rate K_a (1/Ms)	off-rate K_d (1/s)	affinity K_D
Bcl-x_L			
BimSAHB	3.2×10^6	1.5×10^{-1}	45 nM
unstapled BimSAHB	7.9×10^5	7.5×10^{-2}	95 nM
linear BimBH3	1.7×10^6	1.1×10^{-2}	5.7 nM
Mcl-1			
BimSAHB	3.7×10^6	2.7×10^{-3}	0.73 nM
linear BimBH3	4.9×10^6	9.7×10^{-4}	0.20 nM

c	sequence	note
BimSAHB	Ac-^{145}EIWIAQELRXIGDXFNAYYA^{164}-NH_2	X represents linked (*S*)-pentenylalanine residues
BimLOCK	Ac-^{145}EIWIAQELRRIGDEFNAYYA^{164}-NH_2	R154 and E158 linked by lactam bridge
linear BimBH3	Ac-^{145}EIWIAQELRRIGDEFNAYYA^{164}-NH_2	

(a) Competition experiments performed using a Biacore 3000 as previously described.[20] Values are presented as a K_i in nM, with SD (n = 3 independent experiments). (b) Direct affinity measurements for binding of linear BimBH3 and BimSAHB to Bcl-x_L and Mcl-1. Measurements were performed using a BIAcore S51. Peptides were passed over a sensor chip to which either recombinant Bcl-x_L-GST or Mcl-1-GST fusion proteins had been coupled via an anti-GST antibody. Direct association and dissociation rates were measured at a range of concentrations from which K_D values were calculated. Unstapled BimSAHB refers to a BimSAHB peptide in which pentylalanine residues have not been linked. (c) Sequences for peptides.

intimate hydrophobic contact with the side-chain of Phe318, and one of the flanking α-disubstitution methyl groups contacts Gly262. Unexpectedly, enhanced helicity did not improve activity with regards to affinity for the pro-survival proteins or bioactivity, as measured by induction of cytochrome *c* release from mitochondria and cellular uptake. Our findings recapitulate earlier observations[17,18] that stapling of peptides to enforce helicity does not necessarily impart enhanced binding affinity for target proteins and support the notion that interactions between the staple and target protein may be required for high affinity interactions in some circumstances.[19] Thus, the design of stapled peptides should consider how the staple might interact with both the target *and* the rest of the peptide, and particularly in the latter case whether its introduction might disrupt otherwise stabilizing interactions.

In conclusion, we undertook an investigation of stapled peptides as part of our on going studies into the mechanism of the Bcl-2 family of proteins. We found that the addition of a hydrocarbon staple to the BimBH3 peptide, either via Grubbs metathesis or formation of an external amide bond, does not change the peptide-like properties of the molecules in a manner that makes them significantly more drug-like. While modification of peptides may yet prove beneficial for drug development, in this case, we describe that the addition of external constraints does not enhance either binding affinity or cell permeability.

METHODS

Circular Dichroism Measurements. Circular dichroism was used to measure the percentage of helical content for BimSAHB, BimLOCK, and an equivalent linear BimBH3 peptide. Spectra were performed on 50 μM peptide solutions in 0.1 M potassium phosphate (pH 7) at 25 °C. Percent helicity was calculated as previously described.[22,23]

Structure Determination. Bcl-x_L protein preparation, crystallization, and structure determination for both the Bcl-x_L:BimSAHB complex and the Bcl-x_L:BimLOCK complex were as previously described for the Bcl-x_L:BimBH3 complex.[14] Crystallographic statistics for the two complexes are reported in Supplementary Table 1.

Cytochrome *c* Release. Cells were pelleted and lysed in 0.025% (w/v) digitonin containing lysis buffer (20 mM Hepes, pH 7.2, 100 mM KCl, 5 mM $MgCl_2$, 1 mM EDTA, 1 mM EGTA, and 250 mM sucrose, supplemented with Complete Protease Inhibitor Cocktail from Roche). The crude lysates, containing mitochondria, were incubated with or without 1% (w/v) Triton-X100 or increasing concentrations of Bim peptides for 1 h at 30 °C, pelleted at 4000 rpm at 4 °C for 15 min, and the supernatant collected. The amount of released cytochrome *c* was determined by ELISA (R&D systems), according to the manufacturer's protocol.

BIAcore Competition Assays. BIAcore competition assays were performed as previously described.[20,21] Pro-survival proteins (5 nM) (Bcl-2, Bcl-x_L, and Bcl-w prepared as described in ref , Mcl-1 prepared as described in ref 24, A1 prepared as described in ref 25) were incubated with increasing concentrations of BimBH3 peptides for 2 h in running buffer prior to injection onto a CM5 chip onto which either a wild-type 26-mer BimBH3 peptide or an inert BimBH3 mutant peptide (Bim4E) was immobilized.

Direct Affinity Measurements. Direct binding assays were performed with a Biacore S51 as previously described.[9] Briefly, anti-GST antibody was immobilized to a CM5 chip using amine coupling. Recombinant GST-tagged Bcl-x_L or GST-tagged Mcl-1 (100 $\mu g\ mL^{-1}$) was captured to the chip followed by injection of peptide at a variety of concentrations. Sensograms were generated by subtracting the binding response from that of a reference spot to which GST alone had been captured.

Killing Assays. MEFs were trypsinized, collected, and then washed twice in serum-free media followed by plating of cells (5×10^4/well) in 50 μL, exposed to BimSAHB (20 μM) or vehicle in serum-free media for 2 h, and serum replacement (20% (v/v) serum in 50 μL media) for an overall treatment duration as indicated.

Colony Survival Assays. Retroviruses encoding BH3-only proteins were transduced as described.[20] Infected MEFs (GFP(+) cells) were sorted by FACS and long-term assays of colony formation performed as described.[20]

Molecular Modeling. The free energy of interaction between the side-chain groups on the BimBH3-peptide was calculated using the AUTODOCK function.[15] In its original formulation, the AUTODOCK potential (model C) includes terms that represent the entropic

dx.doi.org/10.1021/cb3005403 | ACS Chem. Biol. XXXX, XXX, XXX–XXX

penalty for restriction of conformational freedom and desolvation of the ligand only. Here, we have included these two components for both molecular constituents and consequently reduced the contribution to the total free energy of interaction of each by half. The AMBER all-atom partial atomic charges[26] were used to calculate the electrostatic interaction energy. Hydrogen atoms were added to fill valencies using the UCSF Chimera package.[27]

Detailed methods for peptide synthesis, structure determination, K_i calculations, and binding analysis are provided in the Supporting Information.

■ ASSOCIATED CONTENT

Supporting Information

BimSAHB peptide does not kill MEFs; reconstituted $Bax^{-/-}Bak^{-/-}$ MEF cells express comparable levels of wild-type Bax and Bax K21E. This material is available free of charge via the Internet at http://pubs.acs.org.

Accession Codes

Atomic coordinates and structure factors have been deposited in the Protein Data Bank (PDB ID codes, 2YQ6 for Bcl-xL:BimSAHB and 2YQ7 for Bcl-xL:BimLOCK).

■ AUTHOR INFORMATION

Corresponding Author

*E-mail: Brian.Smith@latrobe.edu.au (B.J.S.); deshayes.kurt@gene.com (K.D.); czabotar@wehi.edu.au (P.E.C.).

Notes

The authors declare the following competing financial interest(s): Genentech is a member of the Roche Group. Roche Pharma and Aileron Therapeutics have an independent collaboration developing stapled peptide technology. Between 2007 and 2010, the Walter and Eliza Hall Institute of Medical Research had a research collaboration agreement with Genentech and Abbott in the field of apoptosis, specifically the Bcl-2 protein family.

■ ACKNOWLEDGMENTS

We thank A. Georgiou, H. Ierino, G. Thompson, and A. Wardak for outstanding technical assistance, P. M. Colman for advice and assistance with manuscript preparation, our colleagues J. Adams, A. Cochran, S. Cory, J. Babon, and V. Dixit for useful discussions, and Abbott Laboratories for ABT-737. This work was supported by fellowships and grants from the Australian Research Council (ARC) (fellowships to T.O. and P.E.C.), the National Health and Medical Research Council (NHMRC) (fellowship to D.C.S.H.; project grants 575561 to P.E.C. and 637360 to P.E.C. and D.C.S.H.; program grants 461221 and 1016701), the Leukemia and Lymphoma Society (LLS) (SCOR 7413), and the Australian Cancer Research Foundation. Infrastructure support from a NHMRC IRIISS grant #361646 and a Victorian State Government OIS grant is gratefully acknowledged (by T.O., H.Y., B.J.S., D.C.S.H, and P.E.C.). X-ray data were collected at the Australian Synchrotron, with assistance from the staff of the macromolecular beamlines.

■ REFERENCES

(1) Tyndall, J. D., Nall, T., and Fairlie, D. P. (2005) Proteases universally recognize beta strands in their active sites. *Chem. Rev. 105*, 973–999.

(2) Bird, G. H., Bernal, F., Pitter, K., and Walensky, L. D. (2008) Synthesis and biophysical characterization of stabilized alpha-helices of BCL-2 domains. *Methods Enzymol. 446*, 369–386.

(3) Walensky, L. D., Kung, A. L., Escher, I., Malia, T. J., Barbuto, S., Wright, R. D., Wagner, G., Verdine, G. L., and Korsmeyer, S. J. (2004) Activation of apoptosis *in vivo* by a hydrocarbon-stapled BH3 helix. *Science 305*, 1466–1470.

(4) Moellering, R. E., Cornejo, M., Davis, T. N., Del Bianco, C., Aster, J. C., Blacklow, S. C., Kung, A. L., Gilliland, D. G., Verdine, G. L., and Bradner, J. E. (2009) Direct inhibition of the NOTCH transcription factor complex. *Nature 462*, 182–188.

(5) LaBelle, J. L., Katz, S. G., Bird, G. H., Gavathiotis, E., Stewart, M. L., Lawrence, C., Fisher, J. K., Godes, M., Pitter, K., Kung, A. L., and Walensky, L. D. (2012) A stapled BIM peptide overcomes apoptotic resistance in hematologic cancers. *J. Clin. Invest. 122*, 2018–2031.

(6) Walensky, L. D., Pitter, K., Morash, J., Oh, K. J., Barbuto, S., Fisher, J., Smith, E., Verdine, G. L., and Korsmeyer, S. J. (2006) A stapled BID BH3 helix directly binds and activates BAX. *Mol. Cell 24*, 199–210.

(7) Oltersdorf, T., Elmore, S. W., Shoemaker, A. R., Armstrong, R. C., Augeri, D. J., Belli, B. A., Bruncko, M., Deckwerth, T. L., Dinges, J., Hajduk, P. J., Joseph, M. K., Kitada, S., Korsmeyer, S. J., Kunzer, A. R., Letai, A., Li, C., Mitten, M. J., Nettesheim, D. G., Ng, S., Nimmer, P. M., O'Connor, J. M., Oleksijew, A., Petros, A. M., Reed, J. C., Shen, W., Tahir, S. K., Thompson, C. B., Tomaselli, K. J., Wang, B., Wendt, M. D., Zhang, H., Fesik, S. W., and Rosenberg, S. H. (2005) An inhibitor of Bcl-2 family proteins induces regression of solid tumours. *Nature 435*, 677–681.

(8) Gavathiotis, E., Suzuki, M., Davis, M. L., Pitter, K., Bird, G. H., Katz, S. G., Tu, H. C., Kim, H., Cheng, E. H., Tjandra, N., and Walensky, L. D. (2008) BAX activation is initiated at a novel interaction site. *Nature 455*, 1076–1081.

(9) Lee, E. F., Chen, L., Yang, H., Colman, P. M., Huang, D. C., and Fairlie, W. D. (2008) EGL-1 BH3 mutants reveal the importance of protein levels and target affinity for cell-killing potency. *Cell Death Differ. 15*, 1609–1618.

(10) Willis, S. N., and Adams, J. M. (2005) Life in the balance: How BH3-only proteins induce apoptosis. *Curr. Opin. Cell Biol. 17*, 617–625.

(11) Dai, H., Smith, A., Meng, X. W., Schneider, P. A., Pang, Y. P., and Kaufmann, S. H. (2011) Transient binding of an activator BH3 domain to the Bak BH3-binding groove initiates Bak oligomerization. *J. Cell Biol. 194*, 39–48.

(12) Skelton, N. J., Chen, Y. M., Dubree, N., Quan, C., Jackson, D. Y., Cochran, A., Zobel, K., Deshayes, K., Baca, M., Pisabarro, M. T., and Lowman, H. B. (2001) Structure-function analysis of a phage display-derived peptide that binds to insulin-like growth factor binding protein 1. *Biochemistry 40*, 8487–8498.

(13) Yang, B., Liu, D., and Huang, Z. (2004) Synthesis and helical structure of lactam bridged BH3 peptides derived from pro-apoptotic Bcl-2 family proteins. *Bioorg. Med. Chem. Lett. 14*, 1403–1406.

(14) Lee, E. F., Sadowsky, J. D., Smith, B. J., Czabotar, P. E., Peterson-Kaufman, K. J., Colman, P. M., Gellman, S. H., and Fairlie, W. D. (2009) High-resolution structural characterization of a helical alpha/beta-peptide foldamer bound to the anti-apoptotic protein Bcl-x(L). *Angew. Chem., Int. Ed. 48*, 4318–4322.

(15) Morris, G. M., Goodsell, D. S., Halliday, R. S., Huey, R., Hart, W. E., Belew, R. K., and Olson, A. J. (1998) Automated docking using a Lamarckian genetic algorithm and an empirical binding free energy function. *J. Comput. Chem. 19*, 1639–1662.

(16) Stewart, M. L., Fire, E., Keating, A. E., and Walensky, L. D. (2010) The MCL-1 BH3 helix is an exclusive MCL-1 inhibitor and apoptosis sensitizer. *Nat. Chem. Biol. 6*, 595–601.

(17) Marshall, G. R., Kuster, D. J., and Che, Y. (2009) Chemogenomics with protein secondary-structure mimetics. *Methods Mol. Biol. 575*, 123–158.

(18) Martin, S. F. (2007) Preorganization in biological systems: Are conformational constraints worth the energy? *Pure Appl. Chem. 79*, 193–200.

(19) Joseph, T. L., Lane, D., and Verma, C. S. (2010) Stapled peptides in the p53 pathway: Computer simulations reveal novel

interactions of the staples with the target protein. *Cell Cycle 9*, 4560–4568.
(20) Chen, L., Willis, S. N., Wei, A., Smith, B. J., Fletcher, J. I., Hinds, M. G., Colman, P. M., Day, C. L., Adams, J. M., and Huang, D. C. S. (2005) Differential targeting of pro-survival Bcl-2 proteins by their BH3-only ligands allows complementary apoptotic function. *Mol. Cell 17*, 393–403.
(21) Lee, E. F., Czabotar, P. E., van Delft, M. F., Michalak, E., Boyle, M., Willis, S. N., Puthalakath, H., Bouillet, P., Colman, P. M., Huang, D. C. S., and Fairlie, W. D. (2008) A novel BH3 ligand that selectively targets Mcl-1 reveals that apoptosis can proceed without Mcl-1 degradation. *J. Cell Biol. 180*, 341–355.
(22) Jackson, D. Y., King, D. S., Chmielewski, J., Singh, S., and Schultz, P. G. (1991) General approach to the synthesis of short alpha-helical peptides. *J. Am. Chem. Soc. 113*, 9391–9392.
(23) Kumita, J. R., Smart, O. S., and Woolley, G. A. (2000) Photo-control of helix content in a short peptide. *Proc. Natl. Acad. Sci. U.S.A. 97*, 3803–3808.
(24) Czabotar, P. E., Lee, E. F., van Delft, M. F., Day, C. L., Smith, B. J., Huang, D. C., Fairlie, W. D., Hinds, M. G., and Colman, P. M. (2007) Structural insights into the degradation of Mcl-1 induced by BH3 domains. *Proc. Natl. Acad. Sci. U.S.A. 104*, 6217–6222.
(25) Smits, C., Czabotar, P. E., Hinds, M. G., and Day, C. L. (2008) Structural plasticity underpins promiscuous binding of the pro-survival protein A1. *Structure 16*, 818–829.
(26) Yang, L., Tan, C.-H., Hsieh, M.-J., Wang, J., Duan, Y., Cieplak, P., Caldwell, J., Kollman, P. A., and Luo, R. (2006) New-generation amber united-atom force field. *J. Phys. Chem. B 110*, 13166–13176.
(27) Pettersen, E. F., Goddard, T. D., Huang, C. C., Couch, G. S., Greenblatt, D. M., Meng, E. C., and Ferrin, T. E. (2004) UCSF Chimera: A visualization system for exploratory research and analysis. *J. Comput. Chem. 25*, 1605–1612.

dx.doi.org/10.1021/cb3005403 | *ACS Chem. Biol.* XXXX, XXX, XXX–XXX

JVI
Journals.ASM.org

Japanese Encephalitis Virus Core Protein Inhibits Stress Granule Formation through an Interaction with Caprin-1 and Facilitates Viral Propagation

Hiroshi Katoh,[a] Toru Okamoto,[a] Takasuke Fukuhara,[a] Hiroto Kambara,[a] Eiji Morita,[b] Yoshio Mori,[d] Wataru Kamitani,[c] Yoshiharu Matsuura[a]

Department of Molecular Virology,[a] International Research Center for Infectious Diseases,[b] and Global COE Program,[c] Research Institute for Microbial Diseases, Osaka University, Osaka, Japan; Department of Virology III, National Institute of Infectious Diseases, Tokyo, Japan[d]

Stress granules (SGs) are cytoplasmic foci composed of stalled translation preinitiation complexes induced by environmental stress stimuli, including viral infection. Since viral propagation completely depends on the host translational machinery, many viruses have evolved to circumvent the induction of SGs or co-opt SG components. In this study, we found that expression of Japanese encephalitis virus (JEV) core protein inhibits SG formation. Caprin-1 was identified as a binding partner of the core protein by an affinity capture mass spectrometry analysis. Alanine scanning mutagenesis revealed that Lys^{97} and Arg^{98} in the α-helix of the JEV core protein play a crucial role in the interaction with Caprin-1. In cells infected with a mutant JEV in which Lys^{97} and Arg^{98} were replaced with alanines in the core protein, the inhibition of SG formation was abrogated, and viral propagation was impaired. Furthermore, the mutant JEV exhibited attenuated virulence in mice. These results suggest that the JEV core protein circumvents translational shutoff by inhibiting SG formation through an interaction with Caprin-1 and facilitates viral propagation *in vitro* and *in vivo*.

In eukaryotic cells, environmental stresses such as heat shock, oxidative stress, UV irradiation, and viral infection trigger a sudden translational arrest, leading to stress granule (SG) formation (1). SGs are cytoplasmic foci composed of stalled translation preinitiation complexes and are postulated to play a critical role in regulating mRNA metabolism during stress via so-called "mRNA triage" (2). The initiation of SG formation results from phosphorylation of eukaryotic translation initiation factor 2α (eIF2α) at Ser^{51} by various kinases, including protein kinase R (PKR), PKR-like endoplasmic reticulum kinase (PERK), general control nonrepressed 2 (GCN2), and heme-regulated translation inhibitor (HRI), which are commonly activated by double-stranded RNA (dsRNA), endoplasmic reticulum (ER) stress, nutrient starvation, and oxidative stress, respectively. Phosphorylation of eIF2α reduces the amount of eIF2-GTP-tRNA complex and inhibits translation initiation, leading to runoff of elongating ribosomes from mRNA transcripts and the accumulation of stalled translation preinitiation complexes. Thus, SGs are defined by the presence of components of translation initiation machinery, including 40S ribosome subunits, poly(A)-binding protein (PABP), eIF2, eIF3, eIF4A, eIF4E, eIF4G, and eIF5. Then, primary aggregation occurs through several RNA-binding proteins (RBPs), including T-cell intracellular antigen-1 (TIA-1), TIA-1-related protein 1 (TIAR), and Ras-Gap-SH3 domain-binding protein (G3BP). These RBPs are independently self-oligomerized with the stalled initiation factors and with other RBPs, such as USP10, hnRNP Q, cytoplasmic activation/proliferation-associated protein-1 (Caprin-1), and Staufen and with nucleated mRNA-protein complex (mRNP) aggregations (3, 4). SG assembly begins with the simultaneous formation of numerous small mRNP granules which then progressively fuse into larger and fewer structures, a process known as secondary aggregation (5). The aggregation of TIA-1 or TIAR is regulated by molecular chaperones, such as heat shock protein 70 (Hsp70) (3), whereas that of G3BP is controlled by its phosphorylation at Ser^{149} (4). SG formation and disassembly in response to cellular stresses are strictly regulated by multiple factors.

Viral infection can certainly be viewed as a stressor for cells, and SGs have been reported in some virus-infected cells. Since the propagation of viruses is completely reliant on the host translational machinery, stress-induced translational arrest plays an important role in host antiviral defense. To antagonize this host defense, most viruses have evolved to circumvent SG formation during infection. For example, poliovirus (PV) proteinase 3C cleaves G3BP, leading to effective SG dispersion and virus propagation (6). Influenza A virus nonstructural protein 1 (NS1) has been shown to inactivate PKR and prevent SG formation (7). In the case of human immunodeficiency virus 1 (HIV-1) infection, Staufen1 is recruited in ribonucleoproteins for encapsidation through interaction with the Gag protein to prevent SG formation (8). In contrast, some viruses employ alternative mechanisms of translation initiation and promote SG formation to limit cap-dependent translation of host mRNA (9, 10). In addition, vaccinia virus induces cytoplasmic "factories" in which viral translation, replication, and assembly take place. These factories include G3BP and Caprin-1 to promote transcription of viral mRNA (11).

Japanese encephalitis virus (JEV) belongs to the genus *Flavivirus* within the family *Flaviviridae*, which includes other mosquito-borne human pathogens, such as dengue virus (DENV), West Nile virus (WNV), and yellow fever virus, that frequently cause significant morbidity and mortality in mammals and birds (12). JEV has

Received 15 August 2012 **Accepted** 15 October 2012
Published ahead of print 24 October 2012
Address correspondence to Yoshiharu Matsuura, matsuura@biken.osaka-u.ac.jp.

doi:10.1128/JVI.02186-12

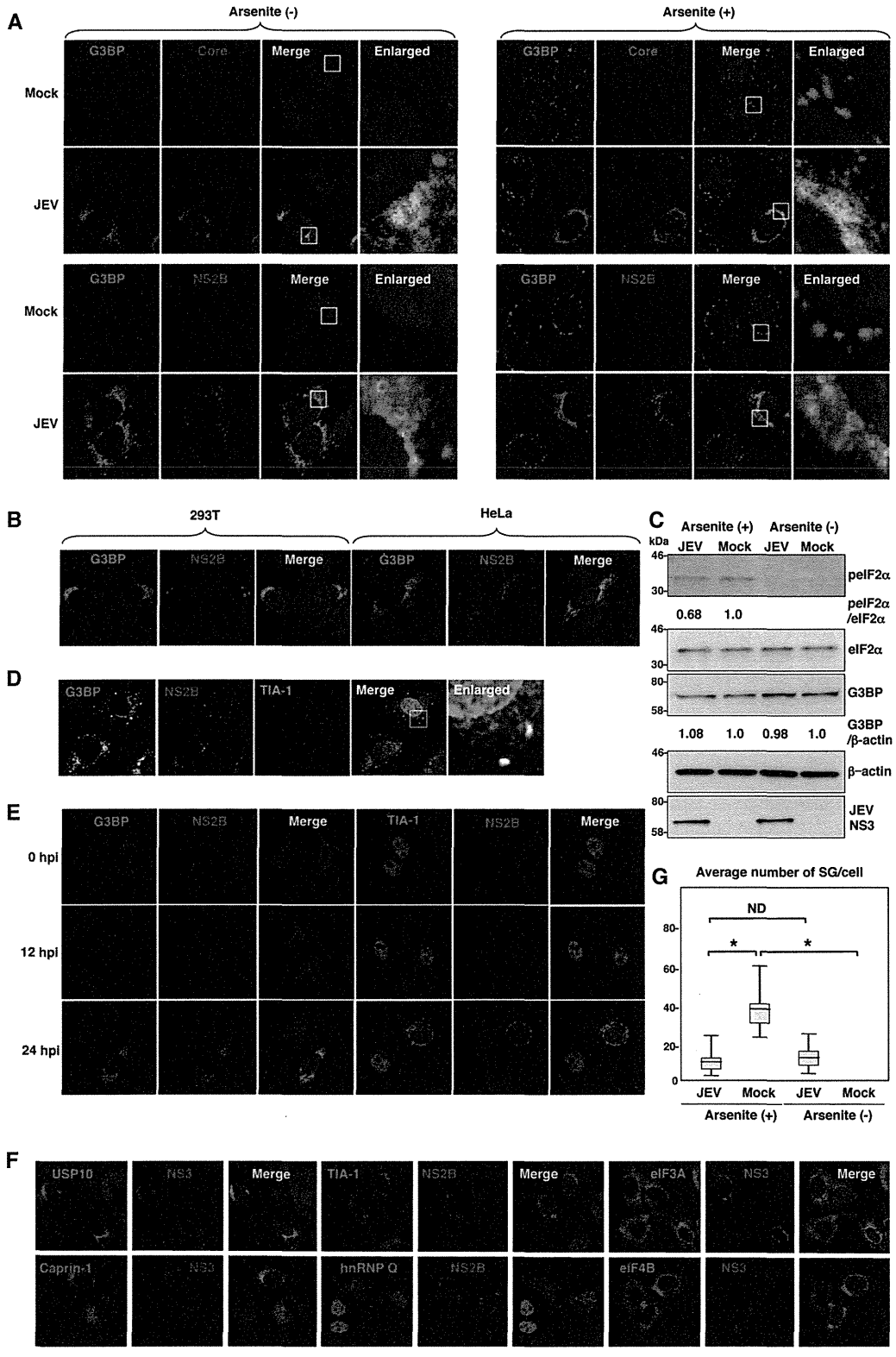

FIG 1 Dynamics of SG-associated factors during JEV infection. (A) Huh7 cells infected with JEV at an MOI of 0.5 were treated with or without 1.0 mM sodium arsenite for 30 min at 37°C, and the levels of expression of G3BP and JEV core protein/NS2B were determined at 24 h postinfection by immunofluorescence analysis with mouse anti-G3BP MAb and rabbit anti-core protein or anti-NS2B PAb, followed by AF488-conjugated anti-mouse IgG (Invitrogen) and AF594-conjugated anti-rabbit IgG, respectively. Cell nuclei were stained with DAPI (blue). (B) Cellular localizations of G3BP and JEV NS2B in 293T and HeLa cells infected with JEV were determined at 24 h postinfection by immunofluorescence analysis with mouse anti-G3BP MAb and rabbit anti-NS2B PAb, followed by AF488-conjugated anti-mouse IgG and AF594-conjugated anti-rabbit IgG, respectively. Cell nuclei were stained with DAPI (blue). (C) Phosphorylation of eIF2α in cells prepared as described in panel A was determined by immunoblotting using the indicated antibodies. The band intensities were quantified by ImageJ

a single-stranded positive-sense RNA genome of approximately 11 kb. The genomic RNA carries a single large open reading frame, and a polyprotein translated from the genome is cleaved co- and posttranslationally by host and viral proteases to yield three structural proteins, the core, precursor membrane (PrM), and envelop (E) proteins, and seven nonstructural (NS) proteins, NS1, NS2A, NS2B, NS3, NS4A, NS4B, and NS5 (13). PrM is further cleaved by the multibasic protease, furin, and matured to membrane (M) protein. The core, M, and E proteins are components of extracellular mature virus particles. NS proteins are not incorporated into particles and are thought to be involved in viral replication, which occurs in close association with ER-derived membranes (14). Previous reports have shown that WNV and DENV inhibit SG formation by sequestering TIA-1 and TIAR through specific interaction with viral RNA (15, 16). In addition, the membrane structure induced by WNV infection was suggested to prevent PKR activation and avoid induction of SG formation (17). In this study, we show that JEV core protein plays an important role in inhibition of SG formation. JEV core protein recruited several SG-associated proteins, including G3BP and USP10, through an interaction with Caprin-1 and suppressed SG formation. Furthermore, a mutant JEV carrying a core protein incapable of binding to Caprin-1 exhibited lower propagation *in vitro* and lower pathogenicity in mice than the wild-type (WT) JEV, suggesting that inhibition of SG formation by the core protein is crucial to antagonize host defense. These results reveal a novel strategy of JEV to inhibit SG formation through an interaction with Caprin-1 and facilitate viral propagation.

MATERIALS AND METHODS

Plasmids. Plasmids encoding FLAG-tagged JEV core protein (pCAGPM-FLAG-Core) and hemagglutinin (HA)-tagged JEV proteins (pCAGPM-HA-JEV proteins) were generated as previously described (18, 19). The cDNA of the core protein of JEV AT31 (amino acid residues 2 to 105) was amplified from the pCAGPM-FLAG-Core plasmid by PCR and cloned into pET21b (Novagen-Merck, Darmstadt, Germany) for expression in bacteria as a His-tagged protein and in pCAG-MCS2-FOS for expression in mammalian cells as a FLAG-One-STrEP (FOS)-tagged protein. The resulting plasmids were designated pET21b-Core-His and pCAG-Core-FOS, respectively. The cDNA of the core protein of DENV2 (amino acid residues 2 to 100) was amplified from the pCAG/FLAG-DEN2C-HA plasmid (19) by PCR and cloned into pCAGPM-N-FLAG. The cDNA of human Caprin-1 was amplified from 293T cells by reverse transcription-PCR (RT-PCR) and cloned into pCAGPM-N-HA (20) and pGEX 6P-1 (GE Healthcare, Buckinghamshire, United Kingdom) for expression in bacteria as a glutathione *S*-transferase (GST) fusion protein and designated pCAGPM-HA-Caprin-1 and pGEX-GST-Caprin-1, respectively. The cDNAs of human G3BP1 and USP10 were also amplified from 293T cells by RT-PCR and cloned into pCAGPM-N-HA. The nucleotide residues of the adenine at 384, adenine at 385, cytosine at 387, and guanine at 388 of the JEV genome in pMWATG1 were replaced with guanine, cytosine, guanine, and cytosine, respectively, by PCR-based mutagenesis to change Lys^{97} and Arg^{98} of the core protein to Ala, yielding pMWAT/KR9798A. The cDNA of the mutant core protein was also cloned into pCAGPM-N-FLAG and pET21b. To generate stable cell lines expressing *Aequorea coerulescens* green fluorescent protein (AcGFP)-fused Caprin-1, the cDNA of human Caprin-1 was amplified by RT-PCR and cloned into pAcGFP N1 (Clontech, Mountain View, CA), and the Caprin-1-AcGFP gene was subcloned into the lentiviral vector pCSII-EF-RfA (21) and designated pCSII-EF-Caprin-1-AcGFP. All plasmids were confirmed by sequencing with an ABI Prism 3130 genetic analyzer (Applied Biosystems, Tokyo, Japan).

Cells and stress treatment. Mammalian cell lines, Vero (African green monkey kidney), 293T (human kidney), Huh7 (human hepatocellular carcinoma), and HeLa (human cervical carcinoma), were maintained in Dulbecco's modified Eagle's minimal essential medium (DMEM) (Sigma, St. Louis, MO) supplemented with 100 U/ml penicillin, 100 mg/ml streptomycin, nonessential amino acids (Sigma), and 10% fetal bovine serum (FBS). The mosquito cell line C6/36 (*Aedes albopictus*) was grown in Leibovitz's L-15 medium with 10% FBS. Huh7 cells were transduced with a lentiviral vector expressing Caprin-1-AcGFP and AcGFP and designated Huh7/Caprin-1-AcGFP and Huh7/AcGFP, respectively. For induction of SGs, cells were treated with sodium arsenite at a final concentration of 1.0 mM in the culture medium for 30 min prior to fixation or lysis of the cells. SG formation was defined morphologically by immunostaining using anti-SG-related factor antibodies described below. Cell viability was determined by using CellTiter-Glo (Promega, Madison, WI) according to the manufacturer's instruction.

Viruses. The wild-type and 9798A mutant of the JEV AT31 strain were generated by the transfection of pMWATG1 and pMWAT/KR9798A, respectively, as described previously (22). Viral infectivity was determined by an immunostaining focus assay as described previously (20), and the results are expressed in focus-forming units (FFU). JEV and DENV serotype 2 New Guinea C strain were amplified in C6/36 cells.

Antibodies. Anti-JEV core rabbit polyclonal antibody (PAb) and anti-JEV NS3 mouse monoclonal antibody (MAb) were prepared as described previously (20, 23). Anti-JEV NS2B rabbit PAb was generated with synthetic peptides of JEV NS2B at Scrum, Inc. (Tokyo, Japan). Anti-DENV core protein rabbit PAb was prepared by using a GST-fused recombinant protein containing amino acid residues 2 to 100 of the DENV core protein. Anti-FLAG mouse MAb (M2) and rabbit PAb and anti-β-actin mouse MAb were purchased from Sigma. Anti-hnRNP Q mouse MAb (ab10687), anti-USP10 rabbit PAb (ab70895), and anti-eIF4B rabbit PAb (ab78916) were purchased from Abcam (Cambridge, United Kingdom). Anti-eIF2α, anti-phospho-eIF2α, and anti-eIF3A rabbit PAbs were purchased from Cell Signaling Technology (Danvers, MA). Anti-HA mouse MAb (HA11), anti-HA rat MAb (3F10), anti-His mouse MAb, anti-GFP mouse MAb (JL-8), anti-JEV envelope protein mouse MAb (6B4A-10), anti-G3BP mouse MAb, anti-TIA-1 goat PAb, anti-Caprin-1 rabbit PAb, and anti-dsRNA mouse MAb were purchased from Covance (Richmond, CA), Roche (Mannheim, Germany), R&D Systems (Minneapolis, MN), Clontech, Chemicon (Temecula, CA), BD Biosciences (Franklin Lakes, NJ), Santa Cruz (Santa Cruz, CA), Proteintech (Chicago, IL), and Bio-

software (NIH, Bethesda, MD), and the relative levels for the indicated proteins are shown based on the level of the mock-infected cells. (D) Cellular localizations of G3BP, NS2B, and TIA-1 in Huh7 cells infected with JEV were determined at 24 h postinfection by immunofluorescence analysis with mouse anti-G3BP MAb, rabbit anti-NS2B PAb, and goat anti-TIA-1 PAb, followed by AF488-conjugated anti-mouse IgG, AF594-conjugated anti-rabbit IgG, and AF633-conjugated anti-goat IgG, respectively. Cell nuclei were stained with DAPI (gray). (E) Dynamics of G3BP and TIA-1 during JEV infection. Huh7 cells infected with JEV were immunostained at 0, 12, and 24 h postinfection (hpi) with mouse anti-G3BP MAb or goat anti-TIA-1 PAb and rabbit anti-NS2B PAb, followed by AF488-conjugated anti-mouse IgG or AF488-conjugated anti-goat IgG and AF594-conjugated anti-rabbit IgG, respectively. Cell nuclei were stained with DAPI (blue). (F) Cellular localization of SG-associated proteins (USP10, Caprin-1, TIA-1, hnRNP Q, eIF3A, and eIF4B) (green, AF488-conjugated secondary antibody) and JEV NS2B/NS3 (red, AF-594-conjugate secondary antibody) in Huh7 cells infected with JEV was determined by immunoblotting at 24 h postinfection. Cell nuclei were stained with DAPI (blue). (G) Numbers of G3BP-positive foci in 30 cells prepared as described in panel A were counted for each experimental condition. Lines, boxes, and error bars indicate the means, 25th to 75th percentiles, and 95th percentiles, respectively. The significance of differences between the means was determined by a Student's *t* test.*, $P < 0.01$; ND, no significant difference.

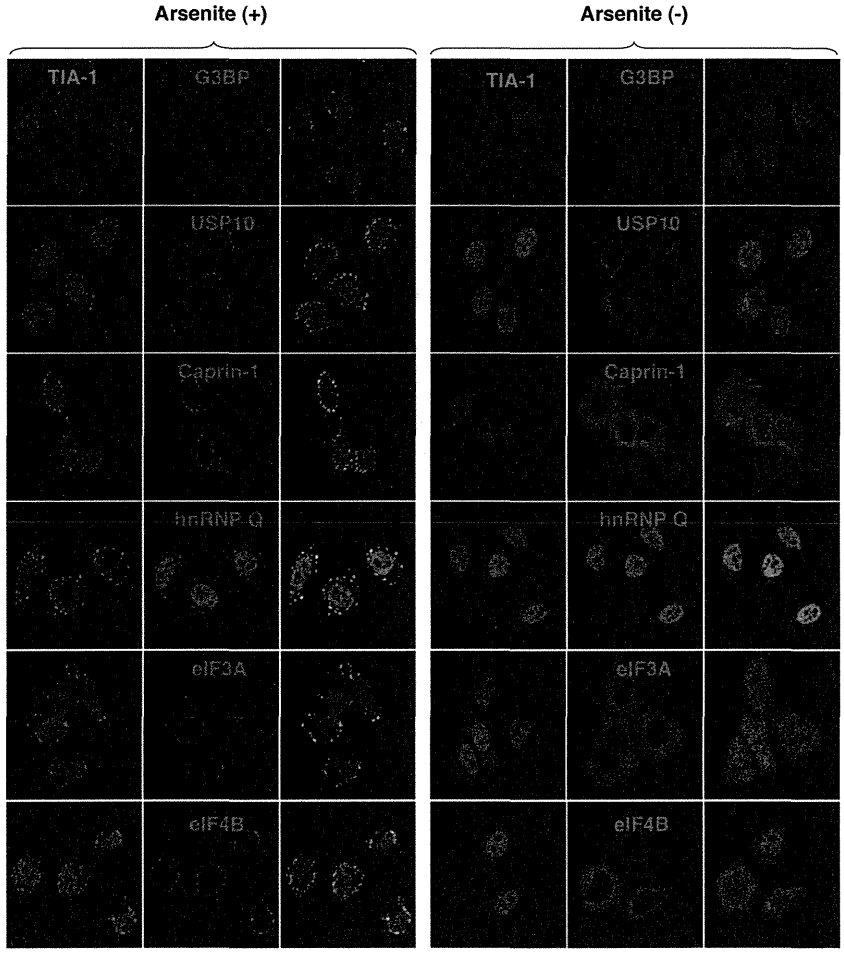

FIG 2 Each SG-associated factor forms SGs under oxidative stress. After treatment with 1.0 mM sodium arsenite for 30 min at 37°C, Huh7 cells were subjected to immunofluorescence analysis with the indicated primary antibodies, followed by AF488-conjugated anti-goat IgG and AF594-conjugated anti-mouse or rabbit IgG. Cell nuclei were stained with DAPI (blue).

center (Szirak, Hungary), respectively. Alexa Fluor (AF)-conjugated secondary antibodies were purchased from Invitrogen (Carlsbad, CA).

Immunofluorescence microscopy. Huh7 cells were fixed in 4% paraformaldehyde in phosphate-buffered saline (PBS) for 15 min at room temperature. After cells were quenched for 10 min with PBS containing 50 mM ammonium chloride (NH_4Cl), they were permeabilized with 0.2% Triton X-100 in PBS for 10 min and blocked with PBS containing 2% bovine serum albumin (BSA) for 30 min at room temperature. The cells were then incubated with the antibodies indicated in the figure legends. Nuclei were stained with 4′,6′-diamidino-2-phenylindole (DAPI). The samples were examined by a Fluoview FV1000 laser scanning confocal microscope (Olympus, Tokyo, Japan).

Transfection, immunoprecipitation, and immunoblotting. Plasmids were transfected into 293T or Huh7 cells by use of TransIT LT1 (Mirus, Madison, WI), and cells collected at 24 h posttransfection were subjected to immunostaining, immunoprecipitation, and/or immunoblotting as described previously (24). The immunoprecipitates were boiled in sodium dodecyl sulfate (SDS) sample buffer and subjected to SDS-polyacrylamide gel electrophoresis (SDS-PAGE). The proteins were transferred to polyvinylidene difluoride membranes (Millipore, Bedford, MA) and incubated with the appropriate antibodies. The immune complexes were visualized with SuperSignal West Femto substrate (Thermo Scientific, Rockford, IL) and detected by use of an LAS-3000 image analyzer system (Fujifilm, Tokyo, Japan).

FOS-tagged purification and mass spectrometry. pCAG-Core-FOS or empty vector was transfected into 293T cells, harvested at 24 h posttransfection, washed with cold PBS, suspended in cell lysis buffer (20 mM Tris-HCl, pH 7.4, 135 mM NaCl, 1% Triton X-100, and protease inhibitor cocktail [Complete; Roche]), and centrifuged at 14,000 × *g* for 20 min at 4°C. The supernatant was pulled down using 50 μl of STrEP-Tactin Sepharose (IBA, Gottingen, Germany) equilibrated with cell lysis buffer for 2 h at 4°C. The affinity beads were washed three times with cell lysis buffer and suspended in 2× SDS-PAGE sample buffer. The proteins were subjected to SDS-PAGE, followed by Coomassie brilliant blue (CBB) staining using CBB Stain One (Nakalai Tesque, Kyoto, Japan). The gels were divided into 10 pieces, and each fraction was trypsinized and subjected to liquid chromatography-tandem mass spectrometry (LC-MS/MS) analysis to identify coimmunoprecipitated proteins. All of the proteins in gels were identified comprehensively, and the proteins detected in cells transfected with pCAG-Core-FOS but not in those with empty vector were regarded as candidates for binding partners of JEV core.

Gene silencing. A commercially available small interfering RNA (siRNA) pool targeting Caprin-1 (siGENOME SMARTpool, human Caprin1) and control nontargeting siRNA were purchased from Dharmacon (Buckinghamshire, United Kingdom) and transfected into 293T cells using Lipofectamine RNAiMAX (Invitrogen) according to the manufacturer's protocol.

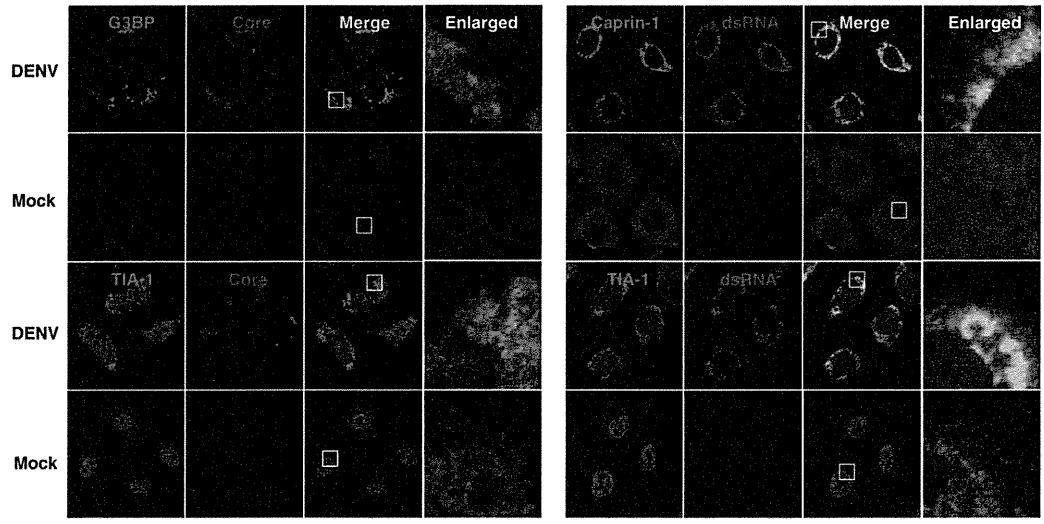

FIG 3 Subcellular localizations of the SG-associated proteins during DENV infection. Cellular localizations of G3BP, Caprin-1, and TIA-1 (green, AF488-conjugated secondary antibody) and viral components (core protein and dsRNA) (red, AF-594-conjugate secondary antibody) in Huh7 cells infected with DENV were determined by immunofluorescence analysis using the appropriate antibodies at 48 h postinfection. Cell nuclei were stained with DAPI (blue).

Preparation of recombinant proteins and GST pulldown assay. His-tagged JEV core protein (core-His) was purified as described in a previous report (25). Briefly, core-His was expressed in *Escherichia coli* (*E. coli*) Rosetta-gami 2(DE3) strain cells (Novagen-Merck) transformed with pET21b-Core-His (WT or 9798A). Bacteria grown to an optical density at 600 nm of 0.6 were induced with 0.5 mM isopropyl-β-D-thiogalactopyranoside (IPTG), incubated for 5 h at 37°C with shaking, collected by centrifugation at 6,000 × *g* for 10 min, lysed in 10 ml of bacteria lysis buffer (50 mM Tris-HCl, pH 7.4, 150 mM NaCl, 1 mM EDTA, 1% Triton X-100, and protease inhibitor cocktail [Complete; Roche]) by sonication on ice, and centrifuged at 10,000 × *g* for 15 min. The supernatant containing core-His was subjected to ammonium sulfate fractionation, followed by cation exchange chromatography with a HiTrap SP column (GE Healthcare). The eluted core-His recombinant protein was dialyzed with 50 mM Tris-HCl buffer containing 150 mM NaCl at 4°C overnight. GST-fused Caprin-1 (GST-Caprin-1) was expressed in *E. coli* BL21(DE3) cells transformed with pGEX-GST-Caprin-1. Bacteria grown to an optical density at 600 nm of 1.0 were induced with 0.1 mM IPTG, incubated for 5 h at 25°C with shaking, collected by centrifugation at 6,000 × *g* for 10 min, lysed in 10 ml of bacteria lysis buffer by sonication on ice, and centrifuged at 10,000 × *g* for 15 min. The supernatant was mixed with 200 μl of glutathione-Sepharose 4B beads (GE Healthcare) equilibrated with bacteria lysis buffer for 1 h at room temperature, and then the beads were washed five times with lysis buffer. Twenty micrograms of GST-Caprin-1 or GST was mixed with equal volumes of the purified core-His for 2 h at 4°C with gentle agitation. The beads were washed five times with bacteria lysis buffer and then suspended in SDS-PAGE sample buffer.

Mouse experiments. Experimental infections were approved by the Committee for Animal Experiment of RIMD, Osaka University (H19-2-0). Female ICR mice (3 weeks old) were purchased from CLEA Japan (Tokyo, Japan) and kept in specific pathogen-free environments. Groups of mice ($n = 10$) were intraperitoneally inoculated with 5×10^4 FFU (100 μl) of the viruses. The mice were observed for 3 weeks after inoculation to determine survival rates. To examine viral growth in the brain, 5×10^4 FFU of the viruses were intraperitoneally administered to the groups of mice ($n = 3$). At 7 days postinfection, mice were euthanized, and the cerebrums were collected. The infectious titers in the homogenates of the cerebrums were determined in Vero cells as described above.

RESULTS

JEV infection confers resistance to SG induction. To examine the formation of SGs in cells infected with JEV, Huh7 cells were infected with JEV at a multiplicity of infection (MOI) of 0.5, and the expression of JEV proteins and an accepted marker for SGs, G3BP, was determined by immunofluorescence analysis at 24 h postinfection. G3BP was mainly accumulated in the perinuclear region and partially colocalized with the JEV core protein, while only partial colocalization with the NS2B protein was also observed (Fig. 1A, left). In addition, a few small G3BP-positive foci were scattered in the cytoplasm. This accumulation of G3BP was observed in not only Huh7 cells but also other cell lines, i.e., 293T and HeLa cells, infected with JEV (Fig. 1B). However, the expression level of G3BP in cells infected with JEV was comparable to that in mock-infected cells (Fig. 1C). To further investigate SG induction by JEV infection, expression of TIA-1, another SG marker, was examined. Although accumulation of TIA-1 in the perinuclear region was not observed, a few TIA-1-positive foci were observed in the JEV-infected cells and were colocalized with G3BP and JEV NS2B, indicating that SG foci were induced in cells infected with JEV (Fig. 1D). The accumulation of G3BP and the aggregation of TIA-1, indicating SG formation, appeared at 24 h postinfection in accord with the expression of viral proteins (Fig. 1E). We further examined the dynamics of other SG-associated factors in cells infected with JEV. Each factor formed clear SGs in cells treated with sodium arsenite, a potent SG inducer eliciting oxidative stress (Fig. 2). As shown in Fig. 1F, three distinct patterns of the subcellular localization of SG components were observed. USP10 and Caprin-1 were accumulated in the perinuclear region and also formed a few small foci scattered throughout the cytoplasm, as seen for G3BP; TIA-1 and hnRNP Q formed cytoplasmic foci but were not accumulated in the perinuclear region; and subcellular localization of eIF3A and eIF4B was not changed. The cytoplasmic foci were confirmed as SGs by immunofluorescence analyses using specific antibodies to SG-associated factors (data not shown). Taken together, these results indicate that JEV infection induces accumulation of several RBPs and formation of a few SGs.

It has been shown previously that infection with WNV or DENV confers resistance to SG formation induced by sodium arsenite (15). To determine the effect of JEV infection on the SG

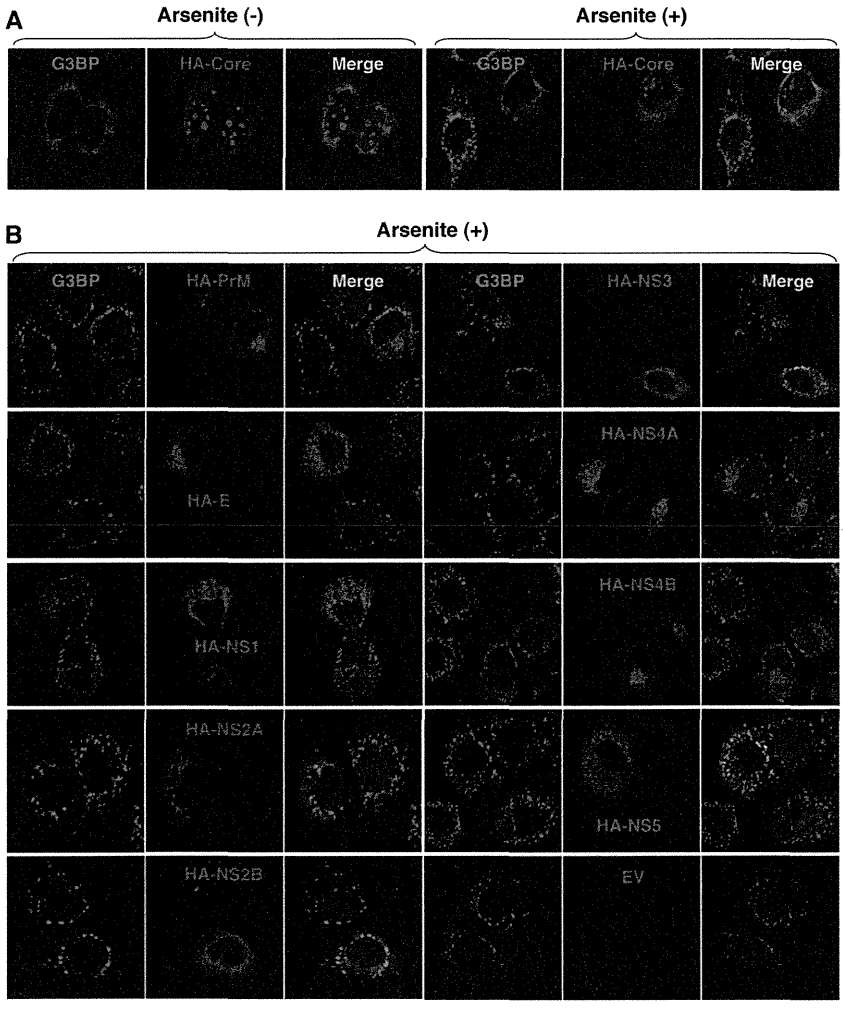

FIG 4 Inhibition of the arsenite-induced SG formation by the expression of JEV proteins. (A) Huh7 cells transfected with a plasmid, pCAGPM-HA-Core, were treated with or without 1.0 mM sodium arsenite for 30 min at 37°C, and the cellular localizations of G3BP and HA-Core were determined at 24 h posttransfection by immunofluorescence analysis with mouse anti-G3BP MAb and rat anti-HA MAb, followed by AF488-conjugated anti-mouse IgG and AF594-conjugated anti-rat IgG, respectively. Cell nuclei were stained with DAPI (blue). (B) Huh7 cells, which were separately transfected with a plasmid expressing an individual viral protein (pCAGPM-HA-JEV protein) as indicated in the figure, were treated with 1.0 mM sodium arsenite for 30 min at 37°C and subjected to an immunofluorescence assay using mouse anti-G3BP MAb and rat anti-HA MAb, followed by AF488-conjugated anti-mouse IgG and AF594-conjugated anti-rat IgG, respectively. Cell nuclei were stained with DAPI (blue).

formation induced by sodium arsenite, JEV-infected cells were treated with 0.5 mM sodium arsenite for 30 min at 24 h postinfection. Although many G3BP-positive foci were observed in mock-infected cells by the treatment with sodium arsenite, accumulation of G3BP in the perinuclear region was observed in the JEV-infected cells (Fig. 1A, right), and the numbers of G3BP-positive foci in the JEV-infected cells were less than those in the mock-infected cells (Fig. 1G). Although it has been reported that a significant reduction of the phosphorylation at Ser^{51} of eIF2α in cells treated with arsenite was induced by infection with WNV (15), the phosphorylation of eIF2α was slightly suppressed in the JEV-infected cells (Fig. 1C). Furthermore, while previous studies reported that Caprin-1 and TIA-1 were colocalized with dsRNA in cells infected with DENV (15, 26), no colocalization of G3BP or TIA-1 with the DENV core protein was observed in the present study (Fig. 3), suggesting that the mechanisms of the viral circumvention of SG formation in cells infected with JEV are different from those in cells infected with WNV and DENV.

JEV core protein suppresses SG formation induced by sodium arsenite. To elucidate the molecular mechanisms of suppression of SG formation induced by sodium arsenite during JEV infection, we tried to identify which viral protein(s) is responsible for the SG inhibition. Since G3BP was colocalized with JEV core protein, we first examined the involvement of the core protein in the perinuclear accumulation of G3BP and in the suppression of SG formation. The expression of JEV core protein alone induced the accumulation of G3BP in the perinuclear region (Fig. 4A, left panel) and suppressed sodium arsenite-induced SG formation (Fig. 4A, upper right cell in the right panel), similarly to JEV infection. In contrast, inhibition of SG formation induced by sodium arsenite was not observed in cells expressing other JEV proteins (Fig. 4B). These results suggest that JEV core protein is responsible for the circumvention of the SG formation observed in cells infected with JEV.

JEV core protein directly interacts with Caprin-1, an SG-associated cellular factor. Since JEV core protein was suggested to